Journal of Physics B: Atomic, Molecular and Optical Physics

PAPER

Low energy inelastic electron scattering from carbon monoxide: I. Excitation of the $a^3\Pi$, $a'^3\Sigma^+$ and $A^1\Pi$ electronic states

To cite this article: Mateusz Zawadzki *et al* 2020 *J. Phys. B: At. Mol. Opt. Phys.* **53** 165201

IOP Publishing Journal of Physics B: Atomic, Molecular and Optical Physics
J. Phys. B: At. Mol. Opt. Phys. **53** (2020) 165201 (20pp) https://doi.org/10.1088/1361-6455/ab95ef

Low energy inelastic electron scattering from carbon monoxide: I. Excitation of the $a^3\Pi$, $a'^3\Sigma^+$ and $A^1\Pi$ electronic states

Mateusz Zawadzki[1,2], Murtadha A Khakoo[1,7], Logan Voorneman[1], Luka Ratkovich[1], Zdeněk Mašín[3], Karel Houfek[3], Amar Dora[4], Russ Laher[5] and Jonathan Tennyson[6]

[1] Physics Department, California State University, Fullerton, CA 92831, United States of America
[2] Atomic Physics Division, Department of Atomic, Molecular and Optical Physics, Gdánsk University of Technology, ul. G. Narutowicza 11/12, 80-233 Gdánsk, Poland
[3] Institute of Theoretical Physics, Faculty of Mathematics and Physics, Charles University, V Holešovičkách 2, 180 00, Prague 8, Czech Republic
[4] Department of Chemistry, North Orissa University, Baripada-757003, Mayurbhanj, Odisha, India
[5] NASA, Exoplanet Science Institute, California Institute of Technology, 1200 E. California Blvd, Pasadena, CA 91125, United States of America
[6] Department of Physics and Astronomy, University College London, London, WC1E 6BT, United Kingdom

E-mail: mkhakoo@fullerton.edu

Received 25 February 2020, revised 5 May 2020
Accepted for publication 22 May 2020
Published 29 June 2020

Abstract

Differential scattering cross sections for electron excitation of the three lowest excited electron states of carbon monoxide are obtained experimentally using low-energy electron energy-loss spectroscopy and theoretically using the *R*-matrix method. The incident electron energies range from near-threshold of 6.3 eV to 20 eV. Experimental scattering angles range from 20° to 120°. The normalization of the experimental cross sections is made to available experimental elastic scattering data (Gibson *et al* 1996 *J. Phys. B: At. Mol. Opt. Phys.* **29** 3197). The *R*-matrix calculations use three distinct close-coupling models and their results are compared to available experimental and theoretical cross sections. The overall comparison leads to significantly improved description of the excitation cross sections for this target.

Keywords: electron scattering, inelastic, molecular excitation

(Some figures may appear in colour only in the online journal)

1. Introduction

Carbon monoxide (CO) plays an important role in various environments [1], for example in combustion of organic molecules, in flames and sparks, in the solar chromosphere, stellar atmospheres and comet tails, in the atmospheres of Venus and Mars [2] and very likely other planets outside our Solar System, in interstellar space, where CO is the second most abundant molecule observed after H_2 [3, 4]. Although CO is not directly involved in global warming effects, its presence very likely affects the abundance of greenhouse gases such as CH_4 and CO_2. Moreover, it is a light molecule and isoelectronic with N_2, therefore it is suitable to theoretical analyses, and it can be obtained in pure form and is readily handled in the laboratory.

The present work examines inelastic electron scattering from CO for electron energies (E_0) from the threshold to $E_0 = 20$ eV. It is aimed to consolidate differential electron

[7] Author to whom any correspondence should be addressed.

scattering cross sections (DCSs) for excitation of the first three lowest excited electronic states of CO, for vibrationally summed electronic states (summed over all vibrational levels in the state) and to compare with available experiments for these states. These vibrationally summed DCSs are then compared to new *R*-matrix computations of these DCSs. The focus here is to look at the electron impact excitation from the $X^1\Sigma^+$ ground state to the three low-lying electronic states, viz the $a^3\Pi$, $a'^3\ \Sigma^+$ and $A^1\Pi$ states, which are the most exposed in an electron energy-loss spectrum. Therefore they can be systematically unfolded from the energy-loss spectrum and thus provide reliable DCS data for theory to model. This region of the spectrum is essentially free of degenerate perturbations since these three states have different symmetries. This also provides a great advantage in the analysis of the electron energy-loss spectrum to provide vibrationally summed DCSs. This is also because the available DCSs near threshold are for excitation of individual vibrational features rather than vibrational summations over whole electronic manifolds, which are needed to compare with theory. This issue is discussed in detail further below. This kind of whole electronic state excitation data is important as a basic starter for guiding theoretical modeling of electron–molecule scattering, and the present work would facilitate a step in the right direction.

There are many data on elastic and inelastic electron scattering from CO which have been currently well-reviewed by Itikawa [4]. We will consider only elastic and inelastic DCS studies pertinent to the present investigation. The latest, most comprehensive experimental work on elastic electron scattering and electron impact vibrational excitation of CO was conducted by Gibson *et al* [5]. Their differential cross sections (DCSs) range from E_0 of 1 eV to 30 eV for scattering angles (θ) ranging from 10° to 130°. They compared their results to earlier works of Ehrhardt *et al* [6], Tanaka *et al* [7] later corrected by Trajmar *et al* [8] to revised He DCSs used in the experiment, Jung *et al* [9], Gote and Ehrhardt [10]; Gibson *et al* provide a comprehensive set of references to previous studies.

There have also been many experimental and theoretical studies of the angle-resolved electronic excitation of CO. The earliest effort was undertaken by Trajmar *et al* [11] using a high energy resolution spectrometer (40 meV, full width at half maximum, FWHM) and an electron energy-loss spectrum unfolding routine developed by them in [12]. They measured vibrationally summed DCSs for the $a^3\Pi$, $a'^3\Sigma^+$, $A^1\Pi$, $b^3\Sigma^+$, $B^1\Sigma^+$, summed $[C^1\Sigma^+ + c^3\Pi]$ and $E^1\Pi$ electronic states at E_0 value of 20 eV [reported in [13]] and further DCSs for excitation of the $a^3\Pi$, $a'^3\Sigma^+$, $A^1\Pi$ states at E_0 values of 12.5 eV and 15 eV reported in Sun *et al* [14]. Soon after, Middleton *et al* [13], using a high resolution spectrometer with an energy-loss resolution of ∼30 to 40 meV, unfolded the energy-loss spectrum of CO in the energy-loss range of around 6 eV to 12 eV and determined vibrationally summed excitation DCSs for the $a^3\Pi$, $a'^3\Sigma^+$, summed $[d^3\Delta + e^3\Sigma^- + I^1\Sigma^- + D^1\Delta]$, $A^1\Pi$, $b^3\Sigma^+$, $B^1\Sigma^+$, $j^3\Sigma^+$, summed $[C^1\Sigma^+ + c^3\Pi]$ and $E^1\Pi$ electronic states using a similar Franck–Condon (FC) spectrum fitting algorithm as [12]. Their DCSs ranged from E_0 values of 20 eV to 50 eV, and θ from 10° to 100°. They compared their results to the DCSs of the distorted-wave calculations of Mu-Tao and McKoy [15]. Overall agreement was unsatisfactory since the data sets differed on average at least by a factor of 2. A detailed, high energy resolution study (20 meV FWHM) of excitation of selected vibrational levels as well as summed vibrational levels of the $a^3\Pi$, $a'^3\Sigma^+$, $d^3\Delta$ and $A^1\Pi$ electronic states was made by Zobel *et al* [16] for E_0 from near-threshold energy to 3.7 eV above the threshold. Their DCSs in many cases are not summed over full electronic-state vibrational manifolds which makes this useful data set not readily comparable with theory or other experimental data sets, and therefore it is an aim of the present work to consolidate it into whole electronic state DCSs. Zobel *et al* [17] also addressed the Rydberg states of CO, i.e. the $b^3\Sigma^+$, $B^1\Sigma^+$, $j^3\Sigma^+$, $C^1\Sigma^+$ and $E^1\Pi$ states for excitation of selected vibrational levels. They compared their results with the Schwinger multichannel variational theory of Sun *et al* [14] and Mu-Tao and McKoy [see [15]] and an eight state *R*-matrix calculation of Morgan and Tennyson [18]. A similar high resolution study was made by Zetner *et al* [19] at the E_0 values of 10 eV, 12.5 eV and 15 eV for vibrationally summed excitation of the $a^3\Pi$, $a'^3\Sigma^+$, $d^3\Delta$ and $A^1\Pi$ states for θ ranging from 9° to 134°. They found excellent agreement with the results of Zobel *et al* [16] which they were able to do after summing the individual vibrational DCSs of [16]. Comparison with theory of [14, 18] showed disagreements regarding the absolute magnitudes of these cross sections.

In addition to the DCS measurements, integral cross-section data have been obtained using an indirect approach measuring electron impact excitation of the $a^3\Pi$ state by detecting the metastable $a^3\Pi$ CO molecules produced. These were done by LeClair *et al* [20] and by Furlong and Newell [21] using different metastable detectors. The two experiments showed disagreement in shape above $E_0 = 10$ eV, but shed light on the influence of cascade processes that feed the $a^3\Pi$ state. Given these discrepancies, and the fact that the past differential scattering data sets did not significantly overlap with each other, we decided to measure electron energy-loss spectra from the near-threshold energy E_0 of 6.3 eV to $E_0 = 20$ eV with the aim of determining vibrationally summed electronic state DCSs and connecting the available experimental excitation DCSs. The present DCSs comprise of vibrationally summed DCSs for the $a^3\Pi$, $a'^3\Sigma^+$, and $A^1\Pi$ states out of a set of DCSs covering also the $d^3\Delta$, $e^3\Sigma^-$, $I^1\Sigma^-$, $D^1\Delta$, $A^1\Pi$, $b^3\Sigma^+$, $B^1\Sigma^+$, $j^3\Sigma^+$, $C^1\Sigma^+$, $c^3\Pi$ and $E^1\Pi$ states, which will be presented in a following paper. These three states are not only the most important of the low-lying states, but are also relatively easier to study. The θ range of the measured DCSs presented is from 10° to 120°; theory, of course, covers all angles but there are also issues with low angle scattering for the dipole allowed excitation of the $A^1\Pi$ state.

In addition to the experimental DCSs we have computed DCSs using the *R*-matrix method at the same energies as the experiment. There are rather few previous theoretical studies of the DCSs for electron impact electronic excitation of CO.

Besides earlier, more limited *R*-matrix studies [5, 18] and studies mentioned above, calculations have also been performed by Lee *et al* [22] who used the Schwinger multichannel method and Machado *et al* [23] using the distorted-wave approximation. It is reasonable to say that none of these theoretical studies obtained particularly good agreement with the measured DCSs. In this work we performed multi-state close-coupling calculations to try to better reproduce the measurements. The use of three distinct models, and two versions of the molecular *R*-matrix codes, allows us to assess the uncertainty of the theoretical results.

2. Method

2.1. Experimental

The apparatus used for the present measurements has been described in earlier papers [24–26], therefore we report here only some aspects of the experiment. The energy-loss spectrometer had both electron monochromator (electron gun) and scattered electron analyzer comprised of 2 cm diameter titanium cylindrical lenses transporting electrons into and out of a double hemispherical energy selector assembly. The system employed a virtual apertures' arrangement and usually performed with an overall energy resolution of 33 to 40 meV, full-width at half-maximum (FWHM) and an incident electron current of 7 to 10 nA. The angular resolution of the analyzer was 2.5° FWHM. Molybdenum collimating apertures were installed in both parts to define the incident electron beam and the scattered electron angle θ. The electron beam from the monochromator intersected a collimated gas beam of CO, formed by the effusive flow of the gas through $a \sim 0.4$ mm diameter aperture of 0.025 mm thickness, located 6 mm below the electron beam axis at the center of the collision region, in a crossed beam geometry. Electrons were detected by a discrete dynode electron multiplier with a dark count-rate of <0.01 Hz [27]. The entire experiment (pumped by a clean-pumping 10″ diameter Diffstak™ diffusion pump equipped with a cold Freon baffle of ≈ -80 °C) was housed in a stainless steel, high vacuum chamber that ran at a base pressure of 1×10^{-7} Torr, and which typically rose to 4×10^{-6} Torr when gas was admitted into the system. The vacuum tank was lined with a dual layer mu-metal shield, which reduced the penetration of magnetic fields into the experiment to about 2 mG. The E_0 value of the beam could range from 0.7 eV to 100 eV, although in this experiment it ran from 6.3 eV to 20 eV. The analyzer had an energy-add lens system that allowed it to detect near-zero scattered electrons. The E_0 scale of the beam was determined with He and calibrated against the well-known He^- 2^2S resonance at 19.366 eV [28]. The analyzer was mounted onto a precise lazy Susan turntable in such a way that it could be located at any θ up to around 120°. The gun and analyzer were both heated by magnetic-field free biaxial resistive heaters [29] to minimize surface contaminants and a clean diffusion pump system ensured a long term stability of the electron beam (>6 months continuous operation). The collimated gas source was mounted on a moveable source arrangement as described by Hughes *et al* [30], wherein the gas beam could be either directed into the electron beam, or rotated away to make background measurements. This setup allows backgrounds to be expediently and accurately measured by effortlessly switching between signal + background (collimated gas beam aligned with the incident electron beam) and background only measurements (collimated gas beam out of alignment with the electron beam). The background spectrum was subtracted from the corresponding signal + background spectrum and the signal spectrum was used in the final analysis described below. Acquisition of electron energy-loss (EEL) spectra was made by the method of multi-channel scaling, repetitively ramping the analyzer's electron energy loss (ΔE) over elastic and inelastic energy-loss features. The configuration of the electronic states covered in this study are given in table 1 and are taken from Krupenie [1], Huber and Herzberg [31], and summarized in Zobel *et al* [16]. Data was typically acquired for approximately 4 to 8 h at each incident energy E_0 and angle θ (including both signal + background and background measurements for equal number of scans), with each data point repeated multiple times for consistency checks. The data acquisition was controlled by a lab computer running Labview™ software, which changed the value of θ at regulated intervals.

Table 1. Electronic configurations of electronic states in the ΔE range of 6 eV to 12 eV, taken from Krupenie [1], Huber and Herzberg [31], and summarized in Zobel *et al* [16].

	Electron configuration									
	Core and valence orbitals							Rydberg orbitals		
State	1σ	2σ	3σ	4σ	1π	5σ	2π	$3s\sigma$	$3p\sigma$	$3p\pi$
$X^1\Sigma^+$	2	2	2	2	4	2				
$a^3\Pi$	2	2	2	2	4	1	1			
$a'^3\Sigma^+$	2	2	2	2	3	2	1			
$d^3\Delta$	2	2	2	2	3	2	1			
$e^3\Sigma^-$	2	2	2	2	3	2	1			
$I^1\Sigma^-$	2	2	2	2	3	2	1			
$A^1\Pi$	2	2	2	2	4	1	1			
$D^1\Delta$	2	2	2	2	3	2	1			
$b^3\Sigma^+$	2	2	2	2	4	1		1		
$B^1\Sigma^+$	2	2	2	2	4	1		1		
$j^3\Sigma^+$	2	2	2	2	4	1			1	
$C^1\Sigma^+$	2	2	2	2	4	1			1	
$a^3\Pi$	2	2	2	2	4	1				1
$E^1\Pi$	2	2	2	2	4	1				1

The procedure for obtaining the normalized cross sections consisted of several steps:

(a) In the first step, the spectrometer was tuned in such a way that the inelastic-to-elastic ratios reproduced closely those from the transmission-free TOF work of LeClair and Trajmar [32] for CO at $\theta = 90°$ which are accurate on a relative scale to ±7%. The result was that over a range of E_0 from 6.5 eV to 20 eV, the inelastic-to-elastic ratios relatively followed the DCSs of the TOF data to within <8%. This served to make the analyzer response roughly within <8% constant as required for unfolding the energy-loss spectra. Since the analyzer was baked and maintained in very

clean vacuum environment this response remained stable, but transmission was checked when starting new E_0 values. At low scattered electron residual energy E_R ($=E_0 - \Delta E$) the transmission was checked using the flat He ionization continuum (to within 10% and was used to correct the EEL spectra [33]). The overall transmission was later re-checked and caused small readjustments to the data, using our own TOF inelastic-to-elastic ratios [34]. This readjustment will be later discussed in more detail. This function was applied to the spectrum obtained at all E_0 values. We accumulated multi-channel energy-loss spectra in the ΔE ranges of -0.15 eV to $+0.15$ eV for elastic and of $+5.750$ eV to $+11.750$ eV for inelastic scattering and for θ of 10° to 120°. These spectra were taken at E_0 values of 6.3 eV, 6.5 eV, 7 eV, 8 eV, 9 eV, 10 eV, 12.5 eV, 15 eV, 17.5 eV and 20 eV. These (essentially background-free) spectra were unfolded to unravel the individual contributions from the vibrational band manifolds of the different electronic states using the method introduced in [36, 37].

(b) The excitation energies ($\Delta E_{n',v'}$), for the electronic state n' and vibrational level v', were determined by an inspection of data from Huber and Herzberg [31], Zobel *et al* [16] for the $X^1\Sigma_g^+$ ($v''=0$) $\rightarrow v'=0$ levels of the a, a′, d, e, I, A, D, b, B, j, C and E states, Zetner *et al* [19] for the $X^1\Sigma_g^+$ ($v''=0$) $\rightarrow v'$ levels of the a, a′, d, e, I, A, D states (taken from their figure 1 and digitized), Hammond *et al* [38] (similarly taken from their digitized figure 4) and Daviel *et al* [39] and by fitting our EEL spectra. After numerous trials of these values to achieve satisfactory test fits to the spectra using our independent vibrational lines algorithm (see (c) below), we were able to obtain excitation energies listed in table 2. The FC factors were determined using Rydberg–Klein–Rees calculations [40] from the Dunham series potential energy curves listed in Huber and Herzberg [31] and were readjusted to fit our spectra at the high E_0 value of 20 eV where the transmission of the spectrometer was expected to be uniform across the 6 eV to 11.5 eV ΔE range. The present excitation energies and FC factors for the states in this range are listed in table 2.

(c) The unfolding procedure has been described in detail in [36, 37]. In this case, the digital multi-channel molecular electron energy loss spectrum of intensity $S(E_0, \theta, \Delta E_i)$ vs ΔE_i corresponding to energy loss ΔE of the 'ith' multichannel bin ($i = 1, 2, \ldots, N$) of the spectrum with $\Delta E_i = \Delta E_1 + (i-1)\delta E$. Here, δE is the energy-loss spectrum's step size per bin; thus for 1000 bins with a range of -0.150 eV to 0.150 eV and jumping to 5.750–11.750 eV, this comprises of $\delta E = 6.306$ meV. It was important that the spectrum was clearly displayed on the computer screen, since a visual display of the fitted energy-loss spectrum and the raw data was found to be a very important and useful component of the unfolding procedure. This digitized ΔE_i scale was determined by using a two-cursor system on the computer graphic display or inputting the start energy loss (of the first bin), ΔE_1, and slope δE of the spectrum using well-known two energy-loss peaks on the spectrum, or a well-known peak and the slope determined from the start ΔE_1 and the end ΔE_N which was logged by the computer from the voltmeter monitoring the spectrometer energy-loss voltage, without incorporating a jump in it. The energy-loss spectrum taken at the fixed E_0 and θ was fitted to the function,

$$S\left(E_0,\theta,\Delta E_i\right) = C\sum_{n'}\sigma_{n'}\left(E_0,\theta\right)\sum_{v'}q_{n',v'} \times F\left(\Delta E_i - \Delta E_{n',v'}\right) + B\left(E_0,\theta,\Delta E_i, I_0\right). \quad (1)$$

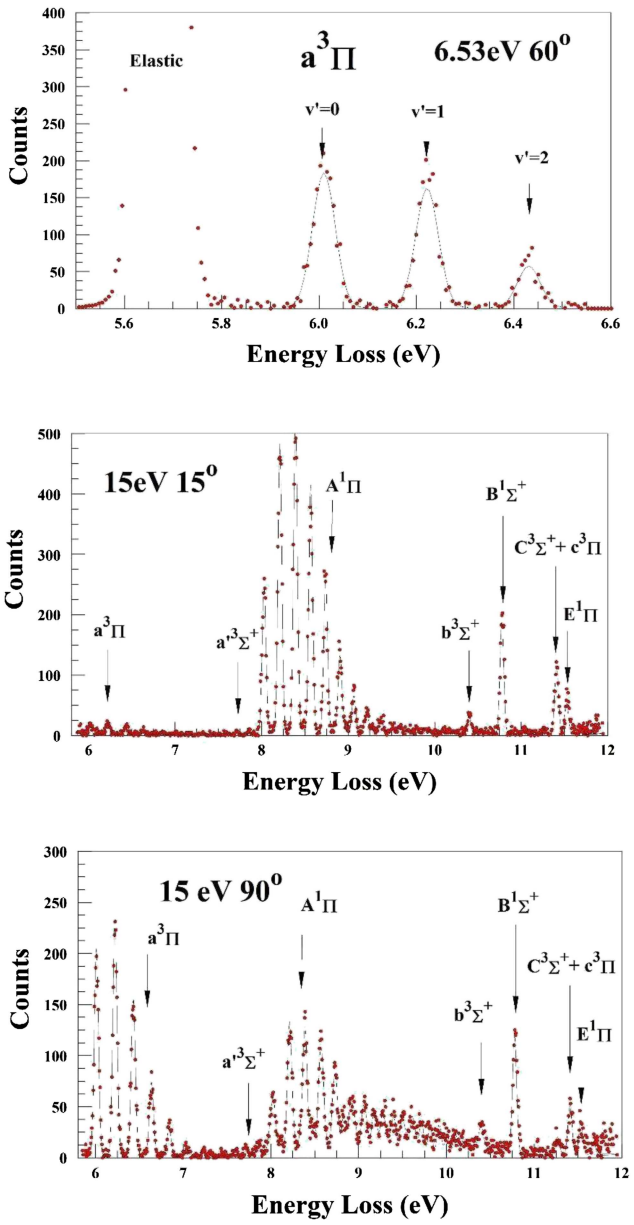

Figure 1. (a)–(c) Electron energy-loss spectra for CO at various E_0 and θ values, showing intensity and positions of excited electronic states from the $X^1\Sigma^+(v''=0)$ ground state. Note (at $E_0 = 15$ eV) the relative rise of the intensity of the $a^3\Pi$ state and the corresponding drop of the intensities of the $a'^3\Sigma^+$ and $A^1\Pi$ states as θ is increased.

Table 2. Excitation energies and Franck-Condon factors for excitation of the $X^1\Sigma^+(v''=0)\rightarrow v'$ vibrational levels of the $a^3\Pi$, $a'^3\Sigma^+$, $d^3\Delta$, $e^3\Sigma^-$, $I^1\Sigma^-$, $A^1\Pi$, $D^1\Delta$, $b^3\Sigma^+$, $B^1\Sigma^+$, $j^3\Sigma^+$, $C^1\Sigma^+$, and $E^1\Pi$ electronic states. The levels in italics were excluded in the unfolding of the electron energy-loss spectra, because they gave a negligible contribution (see text for discussion).

$X^1\Sigma^+(v''=0)\rightarrow v'$	$a^3\Pi$		$a'^3\Sigma^+$		$d^3\Delta$		$e^3\Sigma$		$I^1\Sigma$		$A^1\Pi$	
v′	$E_{\rm loss}$ (eV)	FCF	$E_{\rm loss}$ (eV)	FCF	$E_{\rm loss}$ (eV)	FCF	$E_{\rm loss}$ (eV)	FCF	$E_{\rm loss}$ (eV)	FCF	$E_{\rm loss}$ (eV)	FCF
0	6.01	0.2990	6.851	0.0002	7.497	0.000 0749	7.898	0.0000	8.048	0.0000	8.028	0.1160
1	6.222	03 290	7.001	0.0014	7.64	*0.000 523*	8.034	0.0002	8.180	0.0002	8.211	0.2270
2	6.431	0.2080	7.148	0.0047	7.78	0.001 94	8.168	0.0009	8.311	0.0007	8.391	0.2470
3	6.637	0.0999	7.293	0.0113	7.918	0.005 08	8.299	0.0025	8.438	0.0019	8.567	0.1930
4	6.839	0.0408	7.435	0.0217	8.053	0.0105	8.428	0.0054	8.563	0.0046	8.741	0.1200
5	7.037	0.0150	7.574	0.0354	8.186	0.0185	8.554	0.0098	8.686	0.0091	8.909	0.0608
6	7.231	0.0052	7.711	0.0512	8.316	0.0285	8.678	0.0156	8.806	0.0159	9.076	0.0251
7	*7.422*	*0.0017*	7.846	0.0669	8.444	0.0397	8.801	0.0022	8.924	0.0250	9.242	0.0140
8	*7.609*	*0.0005*	7.979	0.0805	8.569	0.0509	8.921	0.0289	9.040	0.0360	9.407	0.0078
9	*7.793*	*0.0002*	8.109	0.0902	8.693	0.0608	9.039	0.0348	9.153	0.0482	9.572	0.0040
10	*7.973*	*0.0001*	8.237	0.0951	8.814	0.0686	9.156	0.0393	9.264	0.0605	9.738	0.0020
11			8.363	0.0949	8.933	0.0737	9.271	0.0421	9.372	0.0717	*9.905*	*0.000 02*
12			8.487	0.0899	9.049	0.076	9.384	0.0431	9.479	0.0807	*10.074*	*0.000 02*
13			8.609	0.0813	9.163	0.0754	9.496	0.0404	9.583	0.0865	*10.245*	*0.000 01*
14			8.729	0.0702	9.275	0.0725	9.607	0.0404	9.686	0.0886	*10.419*	*0.000 00*
15			8.847	0.0579	9.384	0.0677	9.716	0.0376	9.786	0.0868	*10.594*	*0.000 00*
16			8.964	0.0457	9.492	0.0616	9.824	0.0343	9.900	0.0814	*10.772*	*0.000 00*
17			9.08	0.0345	9.597	0.0548	9.931	0.0308	9.980	0.0731	*10.948*	*0.000 00*
18			9.194	0.0248	9.699	0.0476	10.037	0.0274	10.075	0.0627		
19			9.307	0.0170	9.792	0.0405	10.141	0.0242	10.167	0.0512		
20			9.419	0.0110	9.893	0.0337	10.245	0.0213	10.258	0.0397		
21			9.53	0.0067	9.987	0.0275	10.348	0.0187	10.346	0.0290		
22			9.641	0.0039	10.08	0.0219	10.449	0.0165	10.433	0.0199		
23			9.756	0.0020	10.174	0.017	10.55	0.0145				
24			*9.868*	*0.001*	10.263	0.012	10.645	0.0116				
25			*9.961*	*0.0005*	10.349	0.0089						
26			*10.067*	*0.0003*	10.433	0.0075						
27			*10.162*	*0.000 18*	10.515	0.0055						
28			*10.251*	*0.0001*	10.594	0.0045						
29					10.671	0.0035						
30					10.747	0.003						
Sum FCF		9.99×10^{-1}		1.00		1.00		563×10^{-1}		9.73×10^{-1}		1.01

Table 2. Continued.

$X^1\Sigma^+(v''=0)\rightarrow v'$	$D^1\Delta$		$b^3\Sigma$		$B^1\Sigma$		$j^3\Sigma$		$C^1\Sigma$		$E^1\Pi$	
v′	$E_{\rm loss}$ (eV)	FCF	$E_{\rm loss}$ (eV)	FCF	$E_{\rm loss}$ (eV)	FCF	$E_{\rm loss}$ (eV)	FCF	$E_{\rm loss}$ (eV)	FCF	$E_{\rm loss}$ (eV)	FCF
0	8.107	0.0000	10.396	0.9690	10.776	0.9880	11.270	0.9440	11.408	0.9920	11.517	0.9690
1	8.241	*0.0001*	10.669	0.0314	11.035	0.0117	11.535	0.0515	11.674	0.0081	11.792	0.0312
2	8.371	*0.0004*	*10.943*	*0.0000*	*11.289*	*0.0003*	*11.796*	*0.0040*	*11.925*	2.09×10^{-5}	*12.066*	8.75×10^{-9}
3	8.499	0.0011	*11.216*	*0.0001*	*11.540*	*0.0000*	*12.053*	*0.0050*	*12.184*	6.97×10^{-7}	*12.333*	1.22×10^{-5}
4	8.625	0.0027	*11.489*	*0.0000*	*11.787*	*0.0000*	*12.307*	*0.0001*	*12.439*	4.82×10^{-8}	*12.600*	3.65×10^{-6}
5	8.748	0.0054	*11.760*	*0.0000*	*12.030*	*0.0000*	*12.556*	1.04×10^{-5}	*12.69*	1.56×10^{-9}	*12.865*	4.83×10^{-7}
6	8.868	0.0095			*12.269*	*0.0000*						
7	8.986	0.0149			*12.505*	*0.0000*						
8	9.101	0.0214			*12.736*	*0.0000*						
9	9.214	0.0286			*12.964*	*0.0000*						
10	9.325	0.0360			*13.187*	*0.0000*						
11	9.432	0.0430										
12	9.538	0.0491										
13	9.64	0.0539										
14	9.741	0.0572										
15	9.838	0.0589										
16	9.934	0.0592										
17	10.026	0.0581										
18	10.116	0.0559										
19	10.204	0.0528										
20	10.289	0.0491										
21	10.371	0.0450										
22	10.451	0.0406										
23												
Sum FCF		0.743		1.000		1.000		1.000		1.000		1.000

In this case the normalized (unity sum) instrumental line function,

$$F\left(\Delta E_i - \Delta E_{n',v'}\right) = \sum_{m=1}^{M} \frac{A_m}{\Delta_m\sqrt{\pi}} \exp\left[-\left(\frac{\Delta E_i - \Delta E_{n',v'} + \Delta e_m}{\Delta W_m}\right)^2\right], \tag{2}$$

is a multi-Gaussian function (with m possible up to 5) and with each Gaussian located off the line center $\Delta E_{n',v'}$ by the relative energy loss amount Δe_m and relative intensity A_m and a Gaussian energy width of ΔW_m. Note that in this work we typically employed up to two Gaussians, i.e. $m \leqslant 2$. As aforementioned, $\Delta E_{n',v'}$ is the energy loss value for the v' vibrational level of the n' electronic state obtained from our earlier spectral studies of CO. The spectrometer line function F was synthesized from a multi-Gaussian non-linear squares fit using subroutines from [41] to an isolated energy loss feature, e.g. the $a^3\Pi$ ($v' = 0$, 1, 2) at large θ or the elastic scattering peak at small θ where they are significantly intense. In equation (1) the $q_{n',v'}$ are the FC factors for the vibrational transitions $X^1\Sigma_g$ $(v'' = 0) \rightarrow n'(v')$ in the electronic state vibrational band manifold n' of CO. These $q_{n',v'}$ and $\Delta E_{n',v'}$values are given in table 2. The $\sigma_{n'}(E_0, \theta)$ is the DCS for excitation of the electronic state n'. C is the normalization constant. The function

$$B(E_0, \theta, \Delta E_i, I_0) = \sum_{k=0}^{k<3} B_k \Delta E^k \tag{3}$$

which represented the (secondary electrons) background was expressed as a polynomial of up to order 2 (usually 1) and was dependent on the incident current I_0 and the target density ρ. The variables $\sigma_{n'}(E_0, \theta)$and B_i were determined by a linear least squares fit to the spectrum using subroutines from [41] (note: the $\sigma_{n'}(E_0, \theta)$ will later be determined from the relative $C\sigma_{n'}(E_0, \theta)$ values upon normalization to known cross sections).

We should mention several features in the fitting:

1. The function in equation (1) could be varied nonlinearly to further minimize the residual of the fit. Here the energy loss value of the spectrum at the start of the spectrum, ΔE_1, was changed in successively reduced $\pm$ increments until a minimum in the reduced chi-squared value ($\chi_v{}^2$, where v represents the number of degrees of freedom) was reached. In this procedure, the energy loss step size δE was kept fixed. Importantly, it was observed that the resultant minimum was global for the spectrum.
2. Next the step size δE (=energy loss per unit bin) was also varied in very small $\pm$ amounts in collaboration with (i), to further minimize $\chi_v{}^2$. Steps (i) and (ii) were undertaken concurrently, i.e. if needed step (i) previously described was repeated and followed by (ii), in both cases minimizing the fitting $\chi_v{}^2$. The linearity of the computer ramp voltage (provided by a 10 V, 12 bit digital-to-analog converter) was typically $\pm$ 2 mV in a 5 V span, and the improvements in $\chi_v{}^2$ to the fit were significantly smaller than in (i), since δE did not vary significantly during the experiment. Typical $\chi_v{}^2$ to the fit were in the range of 1–3. A typical unfolded spectra are shown in figures 1(a)–(c). In addition to this we also carried out fits with all the n', v' individual vibrational levels treated as independent components, i.e.:

$$S\left(E_0, \theta, \Delta E_i\right) = C\sum_{n',v'} \sigma_{n'v'}(E_0, \theta) F\left(\Delta E_i - \Delta E_{n',v'}\right) + B(E_0, \theta, \Delta E_i, I_0). \tag{4}$$

Comparisons of both methods were used to determine regular angular distributions for the DCSs for excitation of the summed v' levels of each electronic state. In fact to achieve consistent good agreement between the two methods using equations (1) and (4), we first used equation (4) and allowed the fit to determine the optimal $\chi_v{}^2$ by adjusting the energy loss scale, after which equation (1) was used to determine the best fit with the final determined δE and ΔE_1 values.

(d) At this point the method described by Nickel *et al* [42] was employed to place our total $a^3\Pi + a'^3\Sigma^+ + A^1\Pi + d^3\Delta + e^3\Sigma^- + I^1\Sigma^- + D^1\Delta + A^1\Pi + b^3\Sigma^+ + B^1\Sigma^+ + j^3\Sigma^+ + C^1\Sigma^+ + c^3\Pi + E^1\Pi$ states' intensities on an absolute DCS scale as follows (using the elastic scattering peak taken along with the inelastic electron energy loss features):

1. We corrected the $\Delta E < 5$ eV transmission of the analyzer using the He ionization transmission determined by the procedure in [33] and then the $\Delta E >$ 5 eV transmission using inelastic-to-elastic ratios at $\theta = 90°$ measured in [32] for E_0 values < 8 eV and those measured in our laboratory for E_0 values $\geqslant 8$ eV using our recently built TOF spectrometer [43]. The comparison between our TOF inelastic-to-elastic ratios and those of LeClair and Trajmar [32] showed excellent agreement on average with proportion of our TOF ratios to theirs being 1.07 $\pm$ 0.084 for the ratios from $E_0 = 8$ eV to 20 eV, with the greatest deviation of 1.22 at 17.5 eV (see also table 3 for a listing of these differences in the inelastic-to-elastic ratios between our TOF [34] and those of [32]).
2. Closer to threshold, the FC factors were modified by (see also [36])

$$q^F_{n',v'} = N_{n'}\frac{k_f}{k_i} q_{n',v'}, \tag{5}$$

where k_i ($\sqrt{2m_eE_0}/\hbar$) and k_f ($\sqrt{2m_eE_R}/\hbar$) are the incident and scattered electron momenta, which is essentially an electron flux-factor correction [44]. At energies above 15 eV this correction was not necessary (see also [36]).

(e) The relative intensities of the electronic states were then normalized to the elastic DCSs of Gibson *et al*

Table 3. Our presently determined TOF inelastic-to-elastic ratios R_{Pres} compared to those R_{LeC} of LeClair and Trajmar [32]. Our results are in excellent agreement with [32], except at 17.5 eV. See text for discussion.

E_0 (eV)	R_{Pres}	Error	$R_{\mathrm{pres}}/R_{\mathrm{LeC}}$
8	0.160	0.015	1.02
9	0.205	0.017	0.98
10	0.186	0.015	1.01
12.5	0.103	0.009	1.05
15	0.088	0.007	1.07
17.5	0.080	0.006	1.22
20	0.065	0.006	1.145

[5], which were interpolated between energies not covered by them, using second-order polynomials in E_0 and θ. The choice of Gibson *et al*'s DCSs is very important because, it is the most recent and comprehensive data compilation available and it falls nicely in the range of this work with DCSs at E_0 values of 5 eV, 6 eV, 7.5 eV, 9.9 eV, 15 eV, 20 eV and 30 eV. Using it we were able to accurately interpolate their DCSs to the E_0 values of the present work. Also, this choice was also made after careful comparisons of their DCSs with those of references [6–10]. These comparisons showed that there was best and consistent agreement (within the quoted error bars of $\pm$10%) throughout the data sets (within this E_0 range) between their results and those of Tanaka *et al* [7] revised by Trajmar *et al* [8], using then recent benchmark He DCSs [35] measured by the same group, i.e. the best agreement between any two data sets. Significant disagreements of the Gibson *et al* [5] DCSs were found when comparing with the rest of the elastic scattering DCSs; this excluded them for the present purpose.

The errors in the overall DCSs included fitting errors determined from the error matrix [41] of the fitted parameters (which was dependent on statistical variation of the spectra), ranging from $\approx\pm$4% to 20%, the elastic scattering DCSs from [5] of $\pm$15%, inelastic-to-elastic ratios of $\approx\pm$8% to 10%, thus overall error ranging in quadrature from $\pm$18% to 25%. We also include errors on the FC factors used, estimated to be in the $\pm$10% for E_0 of 6.3 and 6.5 eV, $\pm$8% at E_0 of 8 eV to 10 eV and dropping to $\pm$5% for higher E_0 values. Unlike our earlier spectral analysis in N_2 [36], some rechecking corrections to the DCSs had to be made after the overall fittings using the FC fittings and independent line fittings so that smoother angular distributions resulted. Integral cross sections (ICS) and momentum transfer cross sections (MTCS) are determined from the DCSs by extrapolating the DCSs to small θ and large θ values, using theory as a guide as in [36].

2.2. Theoretical

Below, we report our results based on two distinct R-matrix studies at the equilibrium geometry of CO molecule. The first study used the well-established UKRmol code [45] while the second used the new heavily upgraded UKRmol+ code [46].

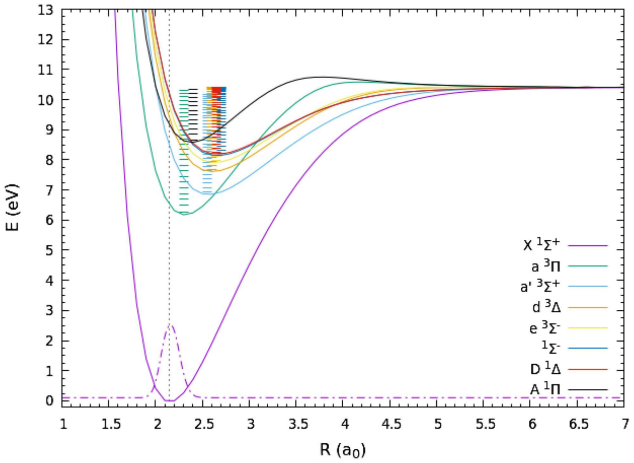

Figure 2. Potential energy curves of CO molecule for the 8 lowest-lying states bound for the equilibrium geometry of the ground state as calculated using the aug-cc-pVQZ basis set and the active space (6,2,2,0), see text for details. The computed vibrational energy levels for each electronic state are indicated as horizontal marks. The dash-dotted curve is the vibrational wave function of the ground neutral state while the vertical dashed line illustrates the difference between the vertical and adiabatic transition from the ground equilibrium geometry.

The main advantage of the UKRmol+ code is the possibility to include B-splines in the representation of the continuum. The earlier UKRmol code only allows the use of Gaussian-type orbitals (GTOs) to represent the continuum. The inclusion of B-splines in UKRmol+ allows one to use arbitrarily large R-matrix radii (useful for calculations which use diffuse representation of the target molecule) and/or higher continuum partial waves than would be possible in the UKRmol calculations. The UKRmol+ code has recently been benchmarked against the molecular convergent close coupling (CCC) method for electron impact electronic excitation of H_2 and found to give excellent results [47]. The improved functionality of new UKRMol+ code proved especially useful in this work for the description of the electronically inelastic dipole-allowed $X^1\Sigma^+ \rightarrow A^1\Pi$ scattering; we show results of calculations including continuum partial waves up to $l = 10$, the largest angular momentum ever explicitly used in a molecular R-matrix calculation. Potential energy curves for 8 lowest-lying electronic states of CO obtained from the UKRmol+ calculations are shown in figure 2. All calculations were performed in C_{2v} symmetry.

2.2.1. UKRmol model. The UKRmol study started from wave functions constructed by two of us to study Feshbach resonances in the 10 to 12 eV region [48]. The CO target at its equilibrium internuclear separation of $2.1323a_0$ was represented by using MOLPRO [49] to generate the state-averaged complete active space self-consistent-field (CASSCF) orbitals using a total of 27 CO target states namely the lowest 4 states of $^1\Sigma^+$, 2 of $^1\Sigma^-$, 4 of $^3\Sigma^+$, 3 of $^3\Sigma^-$, 5 of $^1\Pi$, 5 of $^3\Pi$, 2 of $^1\Delta$ and 2 of $^3\Delta$ symmetry. The CASSCF active space distributes the 10 valence electrons over 10 valence (C_{2v} symmetry) orbitals which were represented using the large cc-pV6Z Gaussian basis set; use of this large basis was found to be important

Table 4. *R*-matrix theory energies obtained from UKRmol+ calculations for excitation of the $X^1\Sigma^+(v''=0) \rightarrow v'$ vibrational levels of the $a^3\Pi$, $a'^3\Sigma^+$, $d^3\Delta$, $e^3\Sigma^+$, $I^1\Sigma^+$, $A^1\Pi$, $D^1\Delta$ electronic states of CO.

v'	$a^3\Pi$	$a'^3\Sigma^+$	$d^3\Delta$	$e^3\Sigma^-$	$I^1\Sigma^-$	$A^1\Pi$	$D^1\Delta$
0	6.173	6.825	7.580	7.876	8.103	8.561	8.150
1	6.377	6.973	7.720	8.011	8.230	8.736	8.276
2	6.580	7.120	7.858	8.145	8.357	8.907	8.401
3	6.778	7.264	7.994	8.275	8.480	9.073	8.522
4	6.973	7.404	8.126	8.402	8.599	9.234	8.640
5	7.164	7.542	8.257	8.527	8.717	9.391	8.756
6	7.353	7.677	8.384	8.650	8.831	9.543	8.869
7	7.537	7.810	8.509	8.769	8.942	9.689	8.978
8	7.718	7.939	8.631	8.886	9.050	9.831	9.085
9	7.895	8.066	8.750	9.001	9.156	9.967	9.188
10	8.069	8.190	8.867	9.112	9.258	10.097	9.288
11	8.240	8.312	8.981	9.221	9.356	10.221	9.385
12	8.407	8.430	9.093	9.327	9.451		9.478
13	8.570	8.547	9.201	9.429	9.543		9.568
14	8.730	8.660	9.307	9.529	9.631		9.653
15	8.886	8.770	9.410	9.626	9.714		9.734
16	9.038	8.878	9.510	9.719	9.792		9.811
17	9.187	8.983	9.607	9.808	9.866		9.883
18	9.332	9.086	9.700	9.894	9.935		9.950
19	9.473	9.185	9.789	9.974	9.998		10.012
20	9.609	9.282	9.875	10.050	10.056		10.069
21	9.741	9.375	9.956	10.121	10.108		10.119
22	9.868	9.465	10.033	10.184	10.154		10.164
23	9.990	9.552	10.103	10.240	10.194		10.202
24	10.107	9.636	10.167	10.284	10.227		10.233
25	10.216	9.716	10.233		10.253		10.258
26		9.792	10.269		10.273		10.277
27		9.865	10.297		10.288		10.290
28		9.933	10.301		10.108		10.299
29		9.996					
30		10.055					

for obtaining a good representation of the higher target states. Details of this calculation are given in reference [48]; the computed excitation energies are presented in table 5 and compare well with the semi-empirical values in table 2.

The scattering calculations were performed at the 27-state close-coupling (CC) level using an *R*-matrix sphere of radius $12a_0$ and continuum functions represented by Gaussian type functions using partial waves up to $l = 4$ (g-waves) [50]. This model gives good results for Feshbach resonances. The positions and widths, as a function of bond distance, of several Feshbach type resonances obtained with this model will be reported elsewhere [51]. The integrated and differential cross sections for various electronic excitations obtained with this model are shown in comparison with the UKRmol+ model and the measured values in section 3. The contribution of higher partial waves ($l > 4$) to the ICSs for the dipole allowed excitation ($X^1\Sigma^+ \rightarrow A^1\Pi$) has been included by using the Born approximation method as employed in the BORNCROSS code [52]. The transition dipole moment value of 2.79 D, obtained by MOLPRO CASSCF calculation for this excitation, was used in evaluating the above Born ICSs correction. However, no such Born correction is applied for the reported DCSs, which therefore is expected to be significantly lower than the measured values at small angles.

2.2.2. UKRmol+ model. The CASSCF calculations performed in MOLPRO [49] used the augmented (i.e. diffuse) and non-augmented (i.e. compact) versions of the cc-pVQZ Gaussian (GTO) atomic basis. The (equilibrium) molecular bond length was set to $2.1a_0$ (1.111 27 Å) which is close to the accurate value 1.112 82 Å [53]. In this case, the 1s orbitals on carbon and oxygen were kept frozen while the active space orbitals comprised the full valence space, i.e. those orbitals occupied in the HF ground state, see table 1, plus the σ^* ($2p_z$), π^* ($2p_x$), π^* ($2p_y$) orbitals of the a_1, b_1 and b_2 C_{2v} irreducible representations. This choice corresponds to the minimal realistic active space capable of describing the lowest-lying electronic states of CO with asymptotes correlating with the lowest-lying excited states of carbon and oxygen. In C_{2v} symmetry used for the actual calculations our configuration-interaction model can be defined as $(1a_1–2a_1)^4$ ($3a_1–6a_1$, $1b_1–2b_1$, $1b_2–2b_2)^{10}$ or (6,2,2,0) and differs from the active space for the UKRmol calculations in the absence of the $3b_1$ and $3b_2$ orbitals in the active space. The state-averaging CASSCF calculation included the first excited

Table 5. Vertical excitation energies in eV for the three lowest excited states of CO obtained from the *R*-matrix models and as a weighted sum of the vibrational experimental thresholds, see text for details. Excitation energies from Nielsen *et al* [54], using experimentally derived spectroscopic data are given for comparison.

State	UKRmol	UKRmol+	Weighted exp.	Observed
$a^3\Pi$	6.43	6.77	6.29	6.32
$a'^3\Sigma^+$	8.36	8.97	8.37	8.51
$A^1\Pi$	9.97	9.46	8.46	8.51

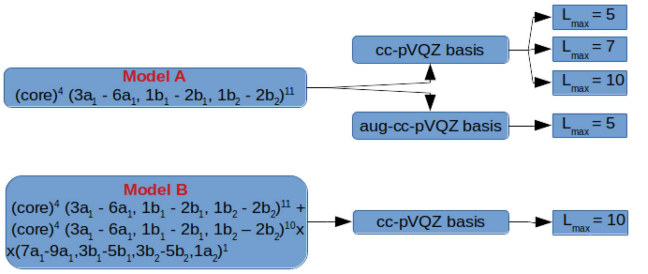

Figure 3. Comparison of models A and B versions of the close-coupling scattering model used in the UKRmol+ calculations. Model B includes the L^2 configurations of model A plus an additional set of configurations based on single excitation from the active space. Here '(core)^4' stands for $(1a_1–2a_1)^4$ The middle box specifies the Gaussian atomic basis used while the boxes on the right show the highest continuum angular momenta included in the calculation. Each combination of the three connected boxes corresponds to parameters of a single calculation.

singlet and triplet state of each Σ, Π and Δ symmetry together with their degenerate C_{2v} components (i.e. a total of 1 + 2 + 2 singlets and 1 + 2 + 2 triplets) plus the ground state and the second triplet Σ excited state resulting in a total of 12 electronic states.

For the purpose of gaining additional insight into our fixed-nuclei calculations we have calculated potential energy curves for the low-lying electronic states of CO using the above mentioned state-averaged CASSCF calculation with the diffuse aug-cc-pVQZ basis set. The resulting curves together with the calculated vibrational levels are shown in figure 2. Clearly, the potential energy curves for the electronically excited states are very steep in the vicinity of the ground state equilibrium geometry: this is illustrated with the help of the vertical dashed line going through the equilibrium geometry. Therefore the vertical excitation energies extracted from the calculations for the equilibrium geometry, see table 5, are not precisely suitable for comparison with the experimental thresholds, especially for the $a'^3\Sigma^+$ state. Nevertheless, as evident from tables 2 and 4, for the two lowest-lying states ($a^3\Pi$, $a'^3\Sigma^+$) the calculated ground vibrational levels ($v' = 0$) are less than 0.2 eV above the experimental ones. In case of the $A^1\Pi$ state the calculated ground vibrational level lies about 0.5 eV above the experimental one. Consequently, we see that our calculations capture the electronic character of the states accurately.

In this work, we carried out UKRmol+ calculations over only a few bond lengths of the molecule (see below), and consequently have not been able to calculate vibrationally resolved cross sections directly comparable with experimental data. For that reason we calculated for each electronic state an average of the experimental vibrational energies weighted by their FC factors. These values constitute our estimate for the weighted thresholds of the electronic states and are also displayed in table 5 and compared to the experimentally derived excitation energies reported in [54], which were determined from the spectroscopic constants in [31] for CO. These resulting weighted thresholds, were then used to shift the calculated UKRmol+ cross section data from the results computed for the vertical thresholds. The potential energy curves show that the equilibrium geometries of the electronically excited states often lie at bond lengths which are non-negligibly larger than the ground-state one and strongly suggesting that an investigation of the dependency of the present fixed-nuclei scattering results on the bond length was necessary.

For the scattering calculations two standard variants of the close-coupling (CC) scattering model [46] were employed both based on the (6,2,2,0) target active space with one electron added into it to represent the L^2 functions modeling correlation/polarization effects due to the electron–molecule interaction (called model A here). In model B an additional set of L^2 functions was added which consisted of single excitations out of the active space to the space of 10 lowest-lying molecular orbitals not included in the active space. Figure 3 shows the schematics of the variants of the models A and B used. In both models a total of 41 lowest-lying electronic states (including the ground state) were included in the CC calculation. The continuum was represented using a mixed B-spline/Gaussian basis centered on the center of mass with the Gaussian exponents up to $l = 6$ taken from our earlier work on BeH [55] and published in [46]. The basis included 20 B-splines starting at $r = 3.5a_0$ and extending up to the *R*-matrix radius ($25a_0$ in case of the calculations with the augmented target basis and $12a_0$ in the non-augmented case). The calculation with the non-augmented target basis was performed for several different choices of the highest partial wave: $l_{max} = 5, 7, 10$. For the calculations with $l_{max} > 6$ only the B-spline part of the continuum included the high-*l* functions: this approach assumes that these higher partial waves do not penetrate significantly into the region $r < 3.5a_0$. Nevertheless, in the region $r < 3.5a_0$ the GTO functions centered on the atoms contribute to the representation of the continuum with $l_{max} > 6$ too. All calculations of the mixed atomic integrals used $\text{Legendre}_{max} = 70$ and $\text{Legendre}_{max} = 65$ in the Legendre (angular momentum) expansion of the 1-electron and 2-electron Coulomb integrals respectively; only for model B we used $\text{Legendre}_{max} = 30$ and observed no artifacts that could be associated with insufficient convergence of the integrals. The calculations for the bond lengths other than the ground state equilibrium one were performed for $R = 2.3a_0$, $R = 2.6a_0$ which correspond roughly to the equilibrium bond lengths of the $^1\Pi$, $^3\Pi$ ($R = 2.3a_0$) and $^3\Sigma^+$ ($R = 2.6a_0$) states. For these calculations model A with $l_{max} = 10$ and the compact cc-pVQZ basis was used.

We observed only negligible differences between the calculations employing the diffuse (aug-cc-pVQZ) and the

Table 6. DCSs, ICS and MTCS and uncertainties (1 standard deviation) for excitation of the $X^1\Sigma^+(v''=0) \rightarrow$ summed v' vibrational levels of the $a^3\Pi$ state at various E_0 and θ (°) values, in units of 10^{-18} cm^2 sr^{-1} (DCSs) and 10^{-18} cm^2 (ICS and MTCS). See text for discussion.

θ (°)	6.3 eV	Error	6.5 eV	Error	7.0 eV	Error	8.0 eV	Error	9.0 eV	Error
10										
15			3.14	0.53	3.82	0.63	5.38	0.89	3.91	0.65
20	1.20	0.36	2.46	0.41	4.12	0.68	6.47	1.07	4.03	0.67
25	1.05	0.32	3.09	0.52	4.11	0.68	5.79	0.96	4.66	0.77
30	1.41	0.42	2.87	0.48	4.56	0.75	6.00	0.99	4.36	0.72
40	1.53	0.46	3.21	0.54	4.65	0.77	5.19	0.86	4.74	0.78
50	1.43	0.43	2.80	0.47	4.63	0.76	5.61	0.93	5.56	0.92
60	1.31	0.39	2.80	0.47	4.25	0.70	6.76	1.11	6.56	1.08
70	1.88	0.56	2.53	0.42	4.07	0.67	6.66	1.10	7.34	1.21
80	1.34	0.40	2.40	0.40	4.07	0.67	7.99	1.32	8.36	1.38
90	1.77	0.53	2.55	0.43	4.55	0.75	7.58	1.25	8.66	1.43
100	1.51	0.45	2.56	0.43	4.55	0.75	10.00	1.65	9.88	1.63
110	1.89	0.57	2.53	0.42	4.37	0.72	11.1	1.8	11.2	1.8
120	1.91	0.57	2.78	0.46	4.61	0.76	12.4	2.0	13.9	2.3
ICS	21.6	7.8	33.7	7.4	57.0	12.0	121.8	24.4	131.7	29.0
MTCS	23.9	7.8	33.2	6.6	59.0	11.1	148.7	26.8	168.0	33.3
θ (°)	10.0 eV	Error	12.5 eV	Error	15 eV	Error	17.5 eV	Error	20 eV	Error
10					0.900	0.153	0.767	0.159	0.495	0.148
15	2.97	0.49	1.29	0.21	0.931	0.154	0.850	0.152	0.575	0.097
20	3.00	0.50	1.31	0.22	0.914	0.151	0.864	0.189	0.656	0.112
25	3.55	0.59	1.42	0.23	0.947	0.156	0.944	0.181	0.700	0.101
30	3.79	0.63	1.63	0.27	1.30	0.21	1.03	0.17	0.755	0.121
40	4.20	0.69	2.06	0.34	1.45	0.24	1.23	0.20	0.910	0.146
50	4.70	0.78	2.26	0.37	1.62	0.27	1.40	0.23	1.03	0.16
60	5.86	0.97	2.69	0.44	2.29	0.38	1.70	0.28	1.13	0.18
70	6.92	1.14	3.25	0.54	2.45	0.40	2.12	0.35	1.27	0.20
80	7.44	1.23	3.73	0.61	3.06	0.50	2.36	0.39	1.35	0.22
90	7.19	1.19	3.51	0.58	2.95	0.49	2.27	0.38	1.45	0.23
100	8.76	1.45	4.02	0.66	2.79	0.46	2.55	0.42	1.82	0.29
110	10.4	1.7	4.8	0.8	3.57	0.59	2.93	0.48	2.15	0.34
120	12.2	2.0	5.6	0.9	3.83	0.63	3.25	0.54	2.45	0.39
ICS	110.0	20.9	51.7	10.3	37.0	7.4	24.1	4.8	22.0	4.4
MTCS	1374.4	23.5	64.5	11.6	44.8	8.1	29.7	5.4	27.8	5.0

compact (cc-pVQZ) basis sets. Therefore the added role of the diffuse GTO functions is small in the present model since it includes only the valence orbitals of the molecule (see table 1) when describing the $a^3\Pi$, $a'^3\Sigma^+$ and $A^1\Pi$ states which are valence states. Consequently, only the results obtained with the computationally expedient cc-pVQZ atomic basis are included in the present discussion. One can expect that the presence of diffuse atomic functions would most likely show up in models that include higher-lying (Rydberg-type) orbitals in the active space to represent higher-lying states e.g. the $b^3\Sigma^+$, $B^1\Sigma^+$, $j^3\Sigma^+$, $C^1\Sigma^+$, $c^3\Pi$ and $E^1\Pi$ states.

We have made detailed calculations with model A ($l_{max} = 10$) and model B for three bond lengths $R = 2.1a_0$, $R = 2.3a_0$, $R = 2.6a_0$. As expected, the features in the cross sections most sensitive to the bond length were connected with formation of resonances. The non-resonant features in the cross sections were not sensitive to the bond length to the extent that would be able to explain the significant differences with respect to the experiment where those appear. Therefore only results computed for the ground equilibrium bond length are included and discussed below.

In the next section we will discuss in detail the results of the UKRmol+ calculations and make a detailed comparison with the experimental data.

3. Results and discussions

3.1. Summary of experimental data

The experimental and theoretical DCSs, ICSs and MTCSs are given in tables 6–8 for the summed v' excitation of the $X^1\Sigma^+(v''=0)$ ground state to the $a^3\Pi$, $a'^3\Sigma^+$ and $A^1\Pi$ states. The DCSs for these states are plotted in figures 4–6, respectively, together with the results of earlier experimental and theoretical works. Similar plots for the ICSs and MTCSs are shown in figure 7.

Table 7. Same as table 6, but for excitation of the $X^1\Sigma^+(v''=0) \rightarrow$ summed v' vibrational levels of the $a'^3\Sigma^+$ state. See text for discussion.

θ (°)	8.0 eV	Error	9.0 eV	Error	10 eV	Error	12.5 eV	Error	15 eV	Error	17.5 eV	Error	20 eV	Error
10									2.24	0.49	1.52	0.67	1.74	0.53
15	0.135	0.030	1.88	0.39	3.74	0.96	3.23	0.65	2.00	0.44	1.48	0.36	1.61	0.48
20	0.0876	0.0193	1.69	0.45	3.81	0.80	2.56	0.51	1.62	0.36	1.30	0.27	1.35	0.44
25	0.0580	0.0128	1.36	0.39	3.36	0.71	1.73	0.35	1.62	0.36	1.09	0.20	1.26	0.37
30	0.0616	0.0135	1.19	0.29	3.05	0.64	1.47	0.29	1.53	0.34	1.14	0.20	1.05	0.26
40	0.0411	0.0090	0.939	0.192	1.97	0.41	1.45	0.29	1.06	0.23	0.916	0.165	0.936	0.178
50	0.0404	0.0089	0.647	0.133	1.64	0.34	1.21	0.24	1.02	0.22	1.02	0.18	0.826	0.157
60	0.0262	0.0058	0.376	0.077	1.41	0.30	1.22	0.24	0.0901	0.198	0.996	0.179	0.583	0.111
70	0.0337	0.0074	0.302	0.062	1.20	0.25	1.23	0.25	0.0916	0.201	0.713	0.128	0.592	0.113
80	0.0316	0.0069	0.216	0.044	0.882	0.185	1.11	0.22	0.896	0.197	0.938	0.169	0.884	0.168
90	0.0390	0.0086	0.174	0.036	0.790	0.166	1.07	0.21	1.21	0.27	1.14	0.20	0.869	0.165
100	0.0484	0.0106	0.175	0.036	0.912	0.191	1.33	0.27	1.26	0.28	1.09	0.20	0.949	0.180
110	0.0429	0.0094	0.228	0.047	0.729	0.153	1.20	0.24	1.39	0.31	0.960	0.173	0.992	0.189
120	0.0408	0.0090	0.381	0.078	1.13	0.24	1.16	0.23	1.56	0.34	1.18	0.21	1.04	0.20
ICS	0.575	0.153	8.52	1.82	18.5	3.8	16.5	3.7	16.8	4.6	13.7	3.3	12.2	2.9
MTCS	0.567	0.143	7.58	1.53	16.0	3.2	15.2	3.2	16.3	4.8	14.5	3.3	13.0	2.6

Table 8. Same as table 4, but for excitation of the $X^1\Sigma^+(v''=0) \rightarrow$ summed v' vibrational levels of the $A^1\Pi$ state. See text for discussion.

θ (°)	9.0 eV	Error	10.0 eV	Error	12.5 eV	Error	15.0 eV	Error	17.5 eV	Error	20.0 eV	Error
10							46.0	9.6	41.6	9.4	43.7	9.0
15	1.61	0.52	5.33	1.06	17.1	2.7	36.2	6.8	32.0	5.4	39.1	6.6
20	1.50	0.34	4.69	0.91	13.1	2.1	24.3	4.7	26.4	4.5	24.6	4.2
25	1.42	0.31	3.97	0.67	11.0	1.8	14.1	2.4	15.9	2.7	14.3	2.4
30	1.24	0.28	3.54	0.60	8.06	1.29	11.1	1.9	9.94	1.69	9.99	1.70
40	1.01	0.18	2.93	0.50	4.84	0.77	4.38	0.75	7.27	1.24	5.00	0.85
50	0.621	0.112	2.43	0.41	3.98	0.64	2.47	0.42	4.03	0.69	3.32	0.56
60	0.557	0.100	2.24	0.38	2.63	0.42	2.34	0.40	3.92	0.67	3.53	0.60
70	0.390	0.070	1.88	0.32	2.93	0.47	2.61	0.44	4.81	0.82	3.86	0.66
80	0.441	0.079	1.81	0.31	2.92	0.47	2.90	0.49	3.70	0.63	2.58	0.44
90	0.401	0.072	1.42	0.24	2.66	0.43	2.72	0.46	3.28	0.56	3.00	0.51
100	0.498	0.090	1.83	0.31	2.42	0.39	2.40	0.41	3.99	0.68	3.12	0.53
110	0.509	0.092	1.96	0.33	2.41	0.39	1.92	0.33	3.14	0.53	3.13	0.53
120	0.524	0.094	2.55	0.43	2.49	0.40	1.77	0.30	2.70	0.46	2.66	0.45
ICS	8.04	1.69	31.9	6.4	46.9	8.9	55.6	11.1	68.1	13.6	62.8	13.2
MTCS	6.10	1.15	31.4	5.7	34.5	5.9	29.6	5.3	44.3	8.0	40.8	7.7

3.2. Excitation of the $a^3\Pi$ state

In figure 4 we show excitation of the $a^3\Pi$ state ($v' = 0,1$) at $E_0 = 6.3$ eV, i.e. 0.3 eV above the threshold 6.010 eV of the vibrational state $v' = 0$ (see table 2). Agreement with all *R*-matrix calculations is equally very good and supports the steep rise in the excitation of this state close to the threshold as a function of E_0. As table 2 shows the Franck–Condon factors for the three lowest vibrational states dominate which allows us to regard even the near-threshold experimental cross sections including transitions up to $v' = 2$ as vibrationally summed and therefore still a fair comparison to a fixed-nuclei theory [56]. At 6.5 eV agreement between experiments (present and Zobel *et al* [16]) is also excellent. The normalization of our DCSs to our TOF values aids significantly in improving the quantitative accuracy of the DCSs for the $a^3\Pi$ state and are in very good agreement with the TOF values at $\theta = 90°$ of LeClair and Trajmar [32], see also table 3, except at $E_0 = 17.5$ eV, where our TOF DCSs are 22% higher. Agreement with the regular UKRmol calculation is somewhat better than with UKRmol+ models A and B. As E_0 is increased, we see all the models (UKRmol, UKRmol+ A and B) in very good agreement with the present experiment, Zobel *et al* [16], Zetner *et al* [19] and Middleton *et al* [13], which are generally in very good agreement with each other. However, at $E_0 = 9$ eV (figure 4(e)), the UKRmol+ models both give DCSs significantly higher than experiments whereas the UKRmol model gives better agreement with the experiments. However, the UKRmol+ models give better agreement with experiments at higher E_0 values of 17.5 eV and 20 eV, especially with the TOF DCSs and those of Middleton *et al* [13] in figure 4(j). When compared with experiments, the present calculations are found to be a significant improvement to those of the Schwinger multichannel ones of Sun *et al* [14].

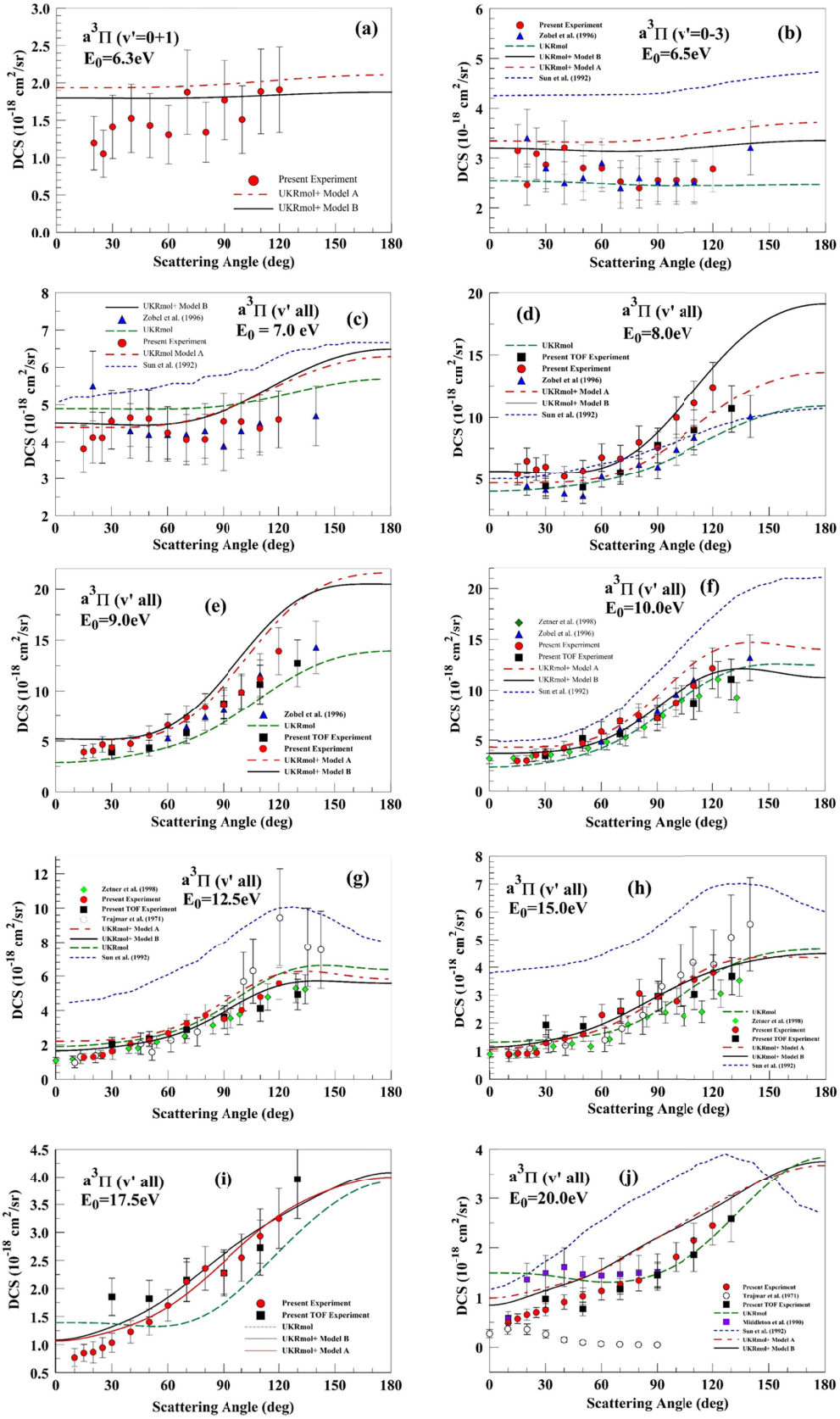

Figure 4. (a)–(j) DCSs for electron impact excitation of the $X^1\Sigma^+(v'' = 0) \rightarrow a^3\Pi$ (all v' states) state of CO at present E_0 values. Legend: experiments: . present experiment using energy-loss spectrometer; ■ present experiment using TOF spectrometer; ▲ Zobel *et al* [16]; ♦ Zetner *et al* [19]; ■ Middleton *et al* [13]; ○ Trajmar *et al* [11, 12]; Theories: _ _ _ (green long dashes) present *R*-matrix model; _ - _ - _ (red long-short dashes) present B-spline *R*-matrix model A and —— (black) model B (see text); - - - (blue short dashes) Schwinger multi-channel variational theory of Sun *et al* [14] (digitized from their graphs). See also discussion in text.

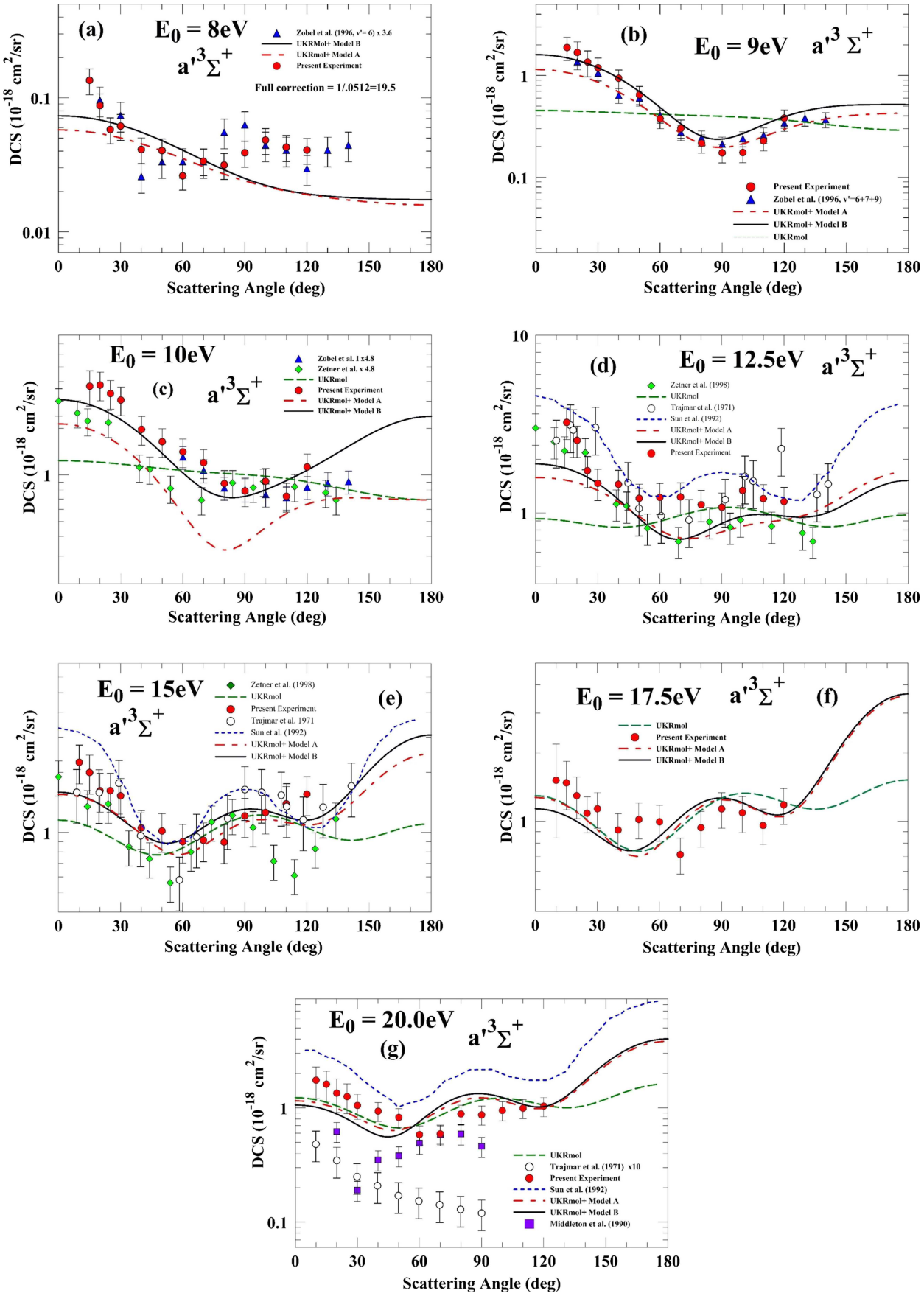

Figure 5. (a)–(g) DCSs for electron impact excitation of the $X^1\Sigma^+(v'' = 0) \rightarrow a'^3\Sigma^+$ (all v' states) state of CO at present E_0 values. Legend is the same as in figure 4. See also discussion in text.

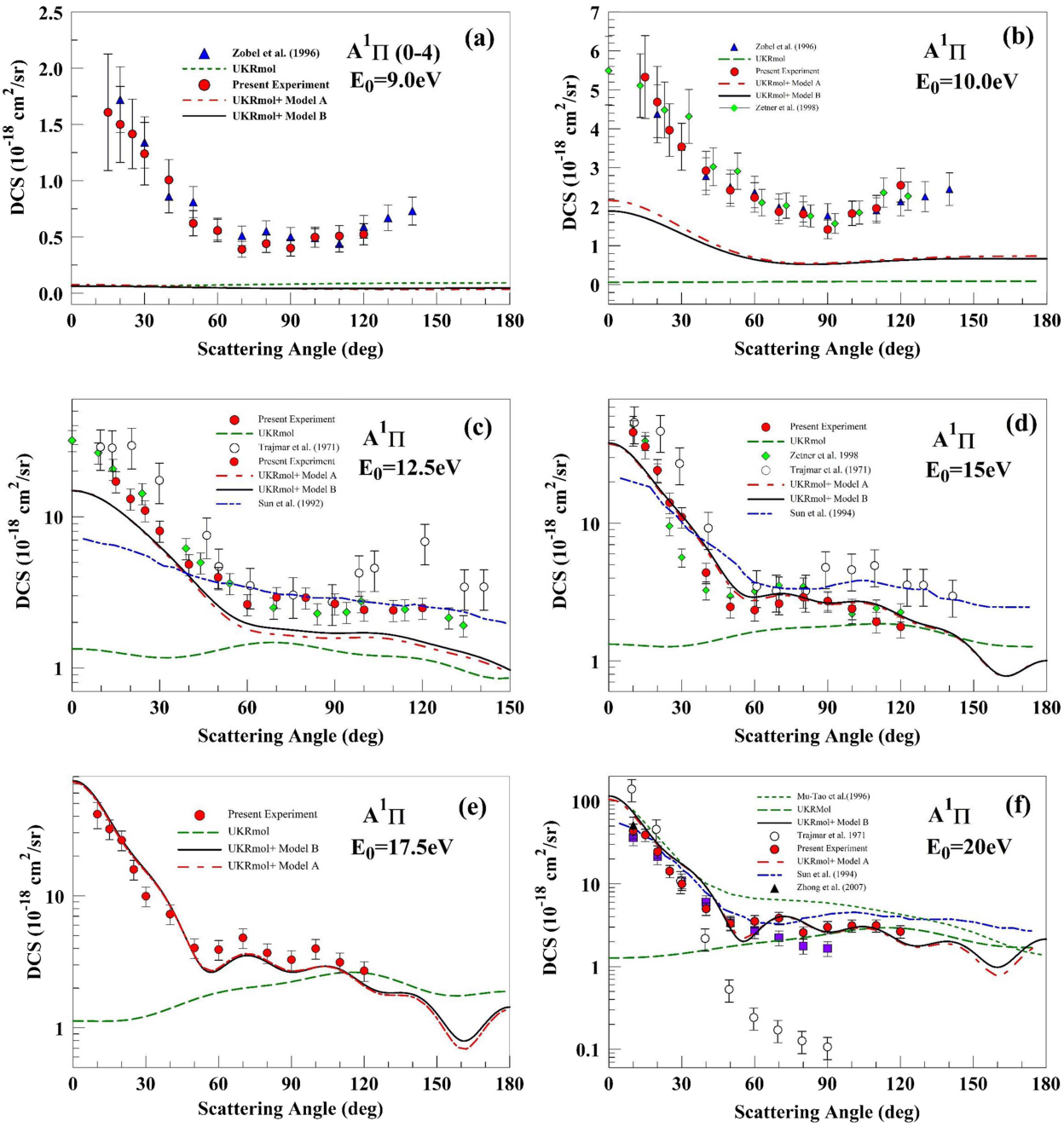

Figure 6. (a)–(f) DCSs for electron impact excitation of the $X^1\Sigma^+(v''=0) \rightarrow A^1\Pi$ (all v' states) state of CO at present E_0 values. Legend is the same as in figure 4, but ---- (green short dashes) Schwinger multi-channel variational theory of Mu-Tao and McKoy [15]. See also discussion in text. The UKRmol+ results (model A and model B) were computed for $L_{max} = 10$ and include the Born correction for higher partial waves. The UKRmol results are for $L_{max} = 4$ and do not contain the Born correction. Also see text for discussion.

Excitation of the $a^3\Pi$ state in the $E_0 = 8$ eV to 10 eV energy range is significantly affected by the $^2\Pi$ resonance centered about 9 eV (see figure 7(a)). Comparing DCSs from UKRmol+ models A and B for this energy range (figures 4(d)–(f)) reveals its effect on the angular distributions. In model B the resonance appears at slightly lower energies (due to the additional L^2 configurations included) and this shift is accompanied by a significant change of backward scattering at 8 eV and 10 eV when compared to model A. This resonance therefore serves as a sensitive probe of correlation/polarization effects included in the calculations. In general, model B agrees better with the experiment therefore we deem it more accurate than model A (see also section 3.2). We already noted that excitation of the $a^3\Pi$ state rises steeply (as a function of E_0). It is spectrally the most isolated state and thus (in principle) easiest to extract its intensity from the energy-loss spectrum as can be seen in figures 1(b) and (c). One would expect both experiment and theory to show the best agreement here for this state because of its strong coupling (via excitation) to the ground state. Figure 1(a) shows that the excitation at threshold is close to the FC factors for excitation of the $a^3\Pi$ v' levels, i.e. supporting the fact that the electronic excitation moment

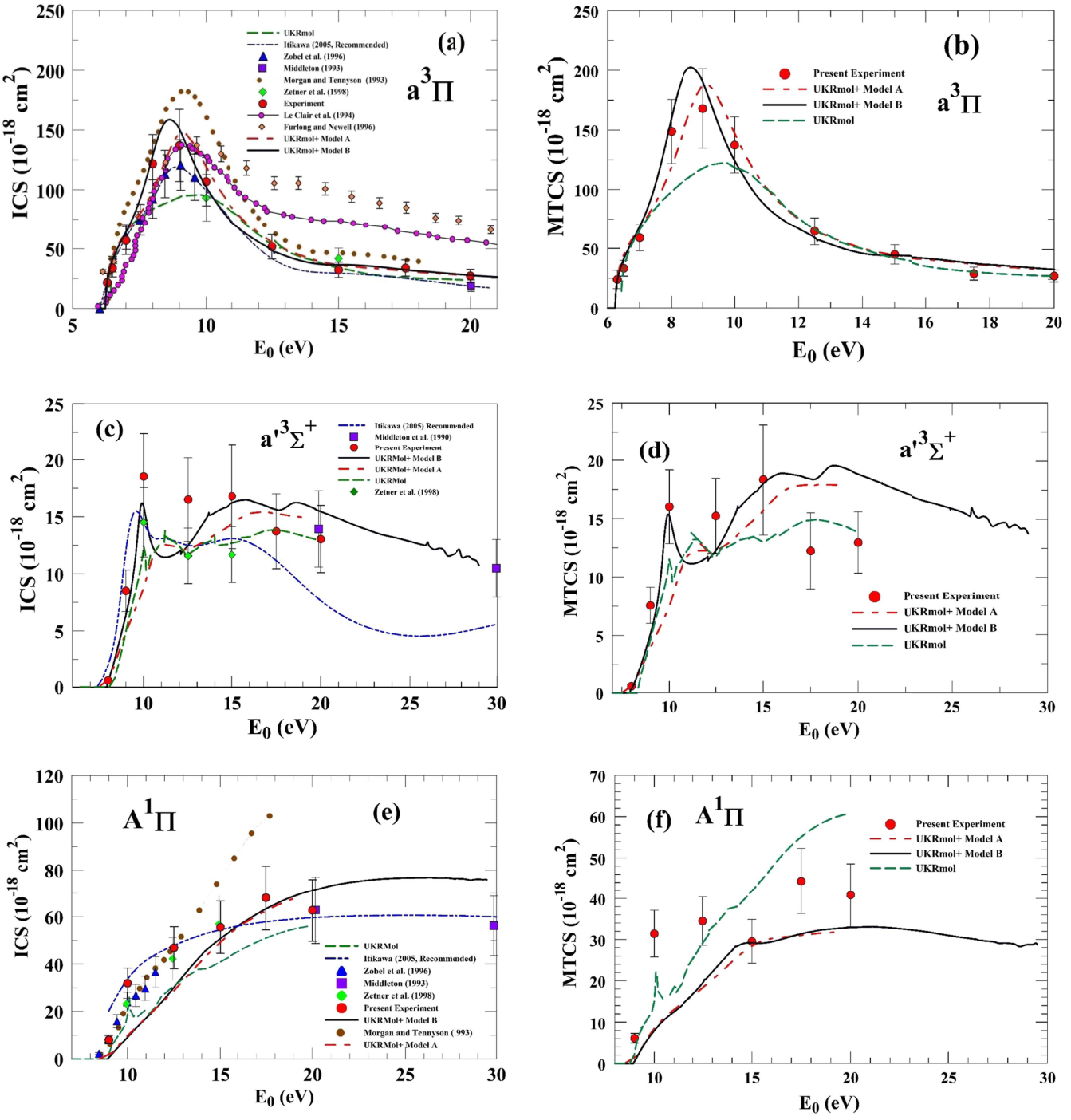

Figure 7. (a)–(f) ICSs and MTCSs for electron impact excitation of the $X^1\Sigma^+(v'' = 0) \rightarrow a^3\Pi$, $a'^3\Sigma^+$, $A^1\Pi$ (all v' states) states as a function of E_0. Legend is the same as in figure 4 except -·-·- (brown) are the ICSs from the *R*-matrix calculations of Morgan and Tennyson [18] and – — – — (purple mixed dashes) are the recommended values by Itikawa in his review article [4]. — • — (pink) and ♦ (brown) are experimental integral cross sections of [20, 21], respectively. See text for discussion.

of this forbidden transition rises rapidly from threshold as can be observed of the ICSs in the figure 7(a).

In figure 7(a), the experimental ICSs show excellent agreement with the UKRmol+ models, but the UKRmol model is quantitatively lower and peaks at a higher energy. The same can be said of the MTCSs in figure 7(b). In figure 7(a), we have included the ICSs for the $a^3\Pi$ state obtained by [20, 21] using detectors that could detect the metastable $a^3\Pi$ state via dimer formation on a frozen Xe layer [20] or surface ionization of the Be–Cu surface by impinging $a^3\Pi$ molecules [21]. The results were corrected for cascading population of the $a^3\Pi$ state by excitation of higher states for energies above 10 eV. One notes that the cascade contributions are quite large, as the 'ICS's determined by these methods show increases in the metastable production of the $a^3\Pi$ state by a factor of 2–3, which is remarkably larger than the ICS for exciting the $a^3\Pi$ state directly.

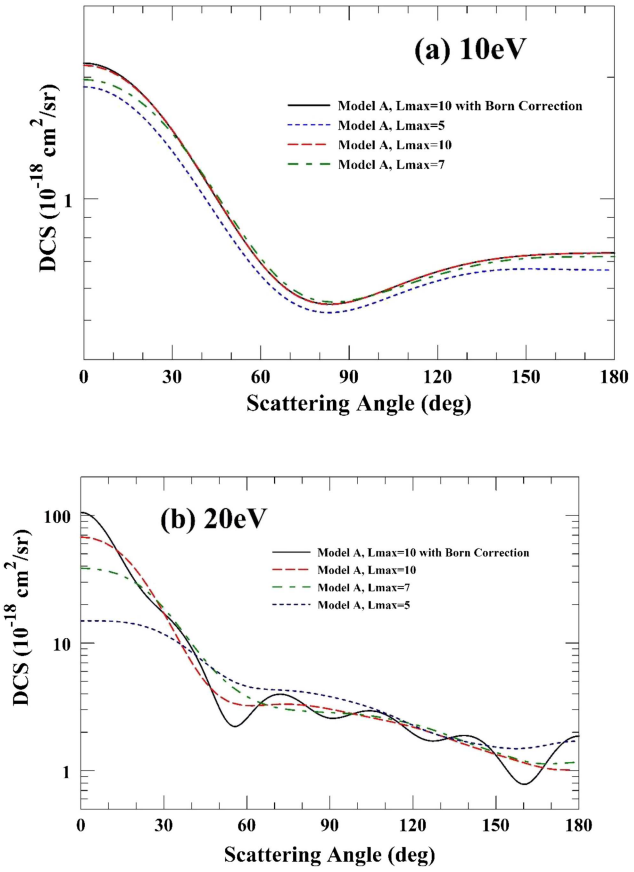

Figure 8. DCSs for (a) $E_0 = 10$ eV and (b) $E_0 = 20$ eV scattering energy and the final $A^1\Pi$ state calculated using UKRmol+ model A and a different number of continuum partial waves included. Legend: ___ (solid line) model A, $L_{max} = 10$ with Born correction; – – – (long red dashes) model A, $L_{max} = 10$; ——–—– (short and long green dashes) model A, $L_{max} = 7$; – – – (short blue dashes) model A, $L_{max} = 5$. The solid lines are results including the Born correction for the higher partial waves. Note the logarithmic scale in these plots.

We see excellent agreement of our experimental ICSs with the UKRmol+ model B for excitation of the $a^3\Pi$ state, but the UKRmol model does not quantitatively agree with experiments at the maximum appearing at the energy of $E_0 = 9$ eV, although it is in very good agreement at higher energies. The ICS of Morgan and Tennyson [18] is somewhat higher at all E_0 values but reproduce the maximum at $E_0 = 9$ eV. Nevertheless the experimental ICSs show very good to excellent agreement with one another.

3.3. Excitation of the $a'^3\Sigma^+$ state

Figures 5(a)–(g) shows the DCSs for the excitation of the $a'^3\Sigma^+$ state from 1 eV above the actual threshold for the $v' = 0$ level. Unlike the $a^3\Pi$ state, equilibrium of the potential energy curve for this state is significantly displaced from the ground $v'' = 0$ vibrational state as can be seen in figure 2 and also discerned from the slow rise of the FC factors in table 2 which peak at $v' = 11$ with the excitation energy of 8.363 eV (8.312 eV in the *R*-matrix calculation). The excitation of this state rises steeply from energies about 8.5 eV as one can see in figure 7(c), i.e. when the higher FC factor members ($v' \geqslant 12$) are engaged. Note that the excitation energy of the lowest $a'^3\Sigma^+(v' = 0)$ level is 6.851 eV, which is below the observed threshold by about 1.65 eV.

We first note that although the $a'^3\Sigma^+$ state is exposed at the $v' \leqslant 8$ levels, its higher vibrational levels overlap with the $A^1\Pi$ state and its unfolding is influenced by intensity of the excitation of the $A^1\Pi$ state, especially at small θ where the contribution of the $A^1\Pi$ state is large (dipole forward scattering). We have made a check on this overlap by adjusting our non-FC (individual lines) with FC fittings to correct for this overlap and find that we had to restrict fittings to FC type fitting based on the exposed $a'^3\Sigma^+$ state for $v' < 8$, especially at small θ, where contributions from the $A^1\Pi$ state raised the DCSs of the $a'^3\Sigma^+$ state by as much as 40%. Figure 5(a) shows the DCSs at 8 eV, where the $v' = 6$ DCS of [16] has to be corrected by a factor 3.6 to compare with us. The full correction would be by a factor 19.5 if all the v' levels of the $a'^3\Sigma^+$ state were open to excitation. The fact that this factor is only 3.6 shows that only part of this manifold is open. Nevertheless, the angular dependence of both experimental DCSs agree very well. As table 2 shows the Franck–Condon factors for the three lowest vibrational states dominate which allows us to regard even the near-threshold experimental cross sections including transitions up to $v' = 2$ as vibrationally summed and therefore still a fair comparison to a fixed-nuclei theory [56]. There is no UKRmol model at this energy, and the UKRmol+ models A and B perform well, but neither of them reproduces the oscillations in the experimental angular distribution. Agreement in DCSs between experiments and the UKRmol+ models is also mostly excellent for all other measured energies (figures 5(b)–(g)) and the UKRmol+ results can be considered as a significant improvement over the results of multichannel Schwinger variational calculations of Sun *et al* [14] at E_0 = 12.5 eV. The experimental DCSs at 9 eV are in excellent agreement with each other, but not with the UKRmol model (here we scaled up the $v' = 6 + 7 + 9$ of Zobel *et al* [16] for best agreement with our DCS).

At $E_0 = 10$ eV (figure 5(c)) we observe that the UKRmol+ model B agrees significantly better with the experiment than model A. Similarly to the case of the $a^3\Pi$ state (see above) this is due to the sensitivity of the DCS to the position of the peak of the $^2\Pi$ resonance which in this case is even sharper and therefore serves as a more sensitive calibration of the theory. Finally, we see that as opposed to the $a^3\Pi$ state channel the resonance in the $a'^3\Sigma^+$ channel enhances the DCS across the whole angular range.

At $E_0 = 15$ eV (figure 5(e)) we see excellent agreement with the very early DCS of Trajmar *et al* reported in [14]. At $E_0 = 17.5$ eV and 20 eV the present results show significant forward scattering enhancement which is pronounced due to the influence of the $A^1\Pi$ state contribution to our unfolding of the spectrum. However, unfolding using profiles forcibly restricted by FC factors to the exposed part of the $a'^3\Sigma^+$ state reduces this rise for the values of $\theta \leqslant 30°$ by a factor of some 40%, improving agreement with all the theoretical *R*-matrix models. The ICSs for the $a'^3\Sigma^+$ state, shown in figure 7(c), also show very good agreement with the *R*-matrix models, deviating for $E_0 \geqslant 10$ eV with the recommended ICSs of Itikawa

[4]. This deviation (i.e. overestimation) can be at least partially attributed to the absence of ionization channels in the *R*-matrix calculations (i.e. two-electron continuum).

3.4. Excitation of the $A^1\Pi$ state

Excitation of this state is the lowest energy dipole-connected electronic state to the ground state. Its threshold is at $E_0 = 8.03$ eV, but it has a slow threshold increase and is first significantly observable at 9 eV for the first 5 v'-levels. Agreement of our experiment with others [13, 16, 19] is very good to excellent across the range of E_0 covered.

The results of the *R*-matrix models do not agree well with the experimental DCSs (see figure 6) and ICS (see figure 7(c)) at the lowest E_0 values of 9 eV, 10 eV and 12.5 eV. We note the good agreement between experiments at these energies, which suggests more a theory problem than an experimental systematic. As expected the DCSs are dominated by the dipole forward scattering peak. Figure 8(a) compares UKRmol+ DCSs at 10 eV obtained with model A for a different number of continuum partial waves. This shows that the disagreement with the experimental ICS at energies below 15 eV is not caused by lack of partial wave convergence in the DCS: the forward peak is actually well converged already for $l_{\max} = 7$ and the contribution of the Born correction is negligible. Additionally, the transition dipole moment with the ground state is 1.70 D. in excellent agreement with the accurate experimental and theoretical value of 1.53 D [57]. We also found that the relative difference between model A and model B for this dipole-allowed transition is negligible (as one can see in figure 6) and the scattering at higher energies (see figure 8(b) for $E_0 = 20$ eV) is heavily dominated by dipole scattering which is not converged *ab initio* even for $l_{\max} = 10$ and in this case a Born correction for higher partial waves must be included. In this work we have extended our DCS code to consider electronic excitation, implemented the Born correction procedure for electronically inelastic transitions using analytic orientation averaging and obtained the Born corrected results within the UKRmol+ model A and model B.

The UKRmol results for the DCSs do not display the forward scattering peak and do not include a Born correction. However, the absence of the Born correction in the UKRmol results does not explain the absence of the forward scattering peak. Instead it is most likely explained by the use of the different model for target description. This also applies to the substantial difference in the transition dipole moments between the UKRmol+ (1.70 D) and UKRmol (2.79 D) calculations. The absence of the forward peak in the UKRmol results then explains the lower magnitude of the integral cross sections in e.g. figure 7(e), which even the larger transition dipole moment is not able to compensate.

The form of the Born correction used for molecules differs to that used for atoms where the full form factor is used while in molecular calculations only the dipole approximation to it has been employed [14, 58–60]. Nevertheless, the full form factor approach has been recently implemented for molecules within the CCC approach [61] and applied to dipole-allowed electronically inelastic transitions in H_2 [62]. The results showed that even when this approach is used the Born DCS for partial waves $l_{\max} > 8$ still manifest significant unphysical oscillations similar to those seen in our figure 8(b). Therefore the use of the dipole approximation to the full form factor is unlikely to be the source of the oscillations seen in our results. However, the Born-corrected Schwinger multichannel results of Sun *et al* [14] do not display the unphysical oscillations in the DCS even for Born corrected results starting with *ab initio* contributions as low as $l_{\max} = 5$ and show only a small sensitivity to $l_{\max}$ [14]. An important difference between the *R*-matrix and CCC approaches on one side and the Schwinger multichannel approach on the other is that the latter uses plane-waves to describe the continuum while the former use partial waves up to some sharp cut off (like $l_{\max} = 10$ in the present UKRmol+ calculations). Therefore in the Schwinger multichannel approach the strong dipolar coupling between the neighboring partial waves ($\Delta l = 1$) is included, at least to some degree, even for large values of continuum angular momenta while in the *R*-matrix and CCC approaches the coupling to partial waves higher than $l_{\max}$ is completely absent. The sharp cut off in our calculations is an approximation which introduces an error into our computed scattering amplitudes. It is possible that it is this error which in combination with the Born *T*-matrix elements produces the unphysical oscillations.

The discussion above shows that the Born correction for higher partial waves of the dipole-allowed electronically inelastic DCS is non-trivial in calculations which use partial wave (rather than plane-wave) representation of the continuum wave function and a dedicated and more detailed study is required to understand its properties fully. This study should also consider the effects of rotational motion which acts to moderate the long-range dipole interactions.

4. Conclusions

We have presented experimental and theoretical vibrationally summed DCSs, ICSs and MTCSs for E_0 values of near-threshold to 20 eV for the electron excitation of the $a^3\Pi$, $a'^3\Sigma^+$ and $A^1\Pi$ electronic states of carbon monoxide from the ground $X^1\Sigma^+(v'' = 0)$ state. In general, improved agreement is found between theory and experiment. The experimental DCSs are in very good to excellent agreement with past measurements and improve the picture for excitation of these important states of CO which produce radiations that are observed in plasma type environments where electrons and CO are present. The use of B-splines in the theory has allowed us to perform the so far highest partial wave *R*-matrix calculations ($l_{\max} = 10$) and obtain converged ICSs for dipole-allowed electronically inelastic transition of the $A^1\Pi$ state at low energies which is a great improvement to the picture in the past. This in turn allowed us to study the accuracy and properties of the dipole approximation to the Born correction for electronically inelastic transitions (for which it is used here for the DCS for the first time). We conclude that our Born correction procedure is insufficient at residual higher energies $\geqslant 6$ eV due to the presence of unphysical oscillations and that either another approach is needed or that simply more

continuum partial waves should be included in such *ab initio* calculations.

The $^2\Pi$ resonance (centered about 9 eV) enhances DCSs for both lowest-lying triplet states in the energy range 8 eV to 10 eV. The experimental DCSs for both states in the vicinity of the resonance serve as a robust and differentiating calibration tool for theoretical models and we used it to calibrate the UKRmol+ theory, selecting model B as the more accurate choice.

The DCSs for the $A^1\Pi$ state are generally converged with respect to partial waves for $l_{max} = 10$ and impact energies < 12.5 eV, i.e. a few eV above the threshold. This shows that the discrepancy between the theory and experiment in this energy range is not due to the dipole interaction but has a different origin, either in the target or polarization description at low E_0 values. It cannot be explained by vibrational averaging of the fixed-nuclei results either due to the small sensitivity of the low-energy cross sections to the bond length.

The present theoretical results (UKRmol+ model B) explain satisfactorily the experiment for the first two states, but the $A^1\Pi$ state at lower energies still poses a challenge for theory. Experimental analysis restricted to FC factors avoids overestimation of the forward scattering for the $a'^3\Sigma^+$ state due to contamination of the signal by the dipole-allowed $A^1\Pi$ state, and shows the sensitivity of added constraints imposed on the fitting using FC functions to represent the $a'^3\Sigma^+$ state and the $A^1\Pi$ state. At higher energies convergence with the number of states included int the close-coupling expansion becomes an issue. Our recent benchmark study on H_2 suggests that the expansions used here should be valid up to the region of the ionization threshold but will tend to overestimate cross sections above this [47]; to achieve convergence at higher energies will require the systematic inclusion of states a possibility which is offered by the *R*-matrix with pseudo-states (RMPS) method [63, 64].

Following this effort we will undertake an examination of the DCSs of the higher Rydberg-valence summed [$d^3\Delta + e^3\Sigma^- + I^1\Sigma^- + D^1\Delta$], $b^3\Sigma^+$, $B^1\Sigma^+$, $j^3\Sigma^+$, summed [$C^1\Sigma^+ + c^3\Pi$] and $E^1\Pi$ electronic states using the present measurements plus supplementary measurements if necessary and future *R*-matrix calculations.

Acknowledgments

MZ acknowledges the Fulbright Program for a senior fellowship to conduct this work at California State University Fullerton. MAK and MZ acknowledge support from National Science Foundation research Grants: NSF-RUI AMO 1606905 and 1911702. KH acknowledges support by the grant agency of the Czech Republic, project GAČR No. 19-20524S. JT thanks the UK EPSRC for funding under the UK-AMOR project, grant EP/R029342/1 and AD acknowledges SERB, Govt. of India grant number EMR/2017/003179. ZM acknowledges support of the grant agency of the Czech Republic, project GAČR Junior No. 20-15548Y and a support of the Charles University project PRIMUS No. 20/SCI/003.

ORCID iDs

Murtadha A Khakoo https://orcid.org/0000-0002-8628-7131
Zdeněk Mašín https://orcid.org/0000-001-9382-4655
Russ Laher https://orcid.org/0000-0003-2451-5482
Jonathan Tennyson https://orcid.org/0000-0002-4994-5238

References

[1] Krupenie P H 1966 *The Band Spectrum of Carbon Monoxide* (*National Standard Reference Series*) (Washington, DC: National Bureau of Standards NSRDS-NBS 5)
[2] Campbell L, Allan M and Brunger M J 2011 *J. Geophys. Res.* **116** A09321
[3] Ehrenfreund P and Cami J 2010 *Cold Spring Harb. Perspect. Biol.* **2** A002097
[4] Itikawa Y 2015 *J. Phys. Chem. Ref. Data* **44** 013105
[5] Gibson J C, Morgan L A, Gulley R J, Brunger M J, Bundschu C J and Buckman S J 1996 *J. Phys. B: At. Mol. Opt. Phys.* **29** 3197
[6] Ehrhardt H, Langhans L, Linder F and Taylor H S 1968 *Phys. Rev.* **173** 222
[7] Tanaka H, Srivastava S K and Chutjian A 1978 *J. Chem. Phys.* **69** 5329
[8] Trajmar S, Register D F and Chutjian A 1983 *Phys. Rep.* **97** 219–356
[9] Jung K, Antoni T, Muller R, Kochem K-H and Ehrhardt H 1982 *J. Phys. B: At. Mol. Phys.* **15** 3535
[10] Gote M and Ehrhardt H 1995 *J. Phys. B: At. Mol. Opt. Phys.* **28** 3957
[11] Trajmar S, Williams W and Cartwright D C 1971 *Proc. 7th Int. Conf. on Electronic and Atomic Collisions* (Amsterdam) (Amsterdam: North-Holland) p 1066 reported in [13].
[12] Trajmar S, Cartwright D C and Williams W 1971 *Phys. Rev.* A **4** 1482
[13] Middleton A G, Brunger M J and Teubner P J O 1993 *J. Phys. B: At. Mol. Opt. Phys.* **26** 1743
[14] Sun Q, Winstead C and McKoy V 1992 *Phys. Rev.* A **46** 6987
[15] Mu-Tao L and McKoy V 1982 *J. Phys. B: At. Mol. Opt. Phys.* **15** 3971
[16] Zobel J, Mayer U, Jung K and Ehrhardt H 1996 *J. Phys. B: At. Mol. Opt. Phys.* **29** 813
[17] Zobel J, Mayer U, Jung K, Ehrhardt H, Pritchard H, Winstead C and McKoy V 1996 *J. Phys. B: At. Mol. Opt. Phys.* **29** 839
[18] Morgan L A and Tennyson J 1993 *J. Phys. B: At. Mol. Opt. Phys.* **2** 2429
[19] Zetner P W, Kanik I and Trajmar S 1998 *J. Phys. B: At. Mol. Opt. Phys.* **31** 2395
[20] LeClair L R, Brown M D and McConkey J W 1994 *Chem. Phys.* **189** 769
[21] Furlong J M and Newell W R 1996 *J. Phys. B: At. Mol. Opt. Phys.* **29** 331
[22] Lee M-T, M Machado A, Fujimoto M M, Machado L E and Brescansin L M 1996 *J. Phys. B: At. Mol. Opt. Phys.* **29** 4285
[23] Machado L E, Mu-Tao L, Brescansin L M, Lima M A P and McKoy V 1995 *J. Phys. B: At. Mol. Opt. Phys.* **28** 467
[24] Khakoo M A, Beckmann C E, Trajmar S and Csanak G 1994 *J. Phys. B: At. Mol. Opt. Phys.* **27** 3159
[25] Varela K, Hargreaves L, Ralphs K, Khakoo M A, Winstead C, McKoy V V, Rescigno T and Orel A 2015 *J. Phys. B: At. Mol. Opt. Phys.* **48** 115208
[26] Ralphs K, Serna G, Hargreaves L, Khakoo M A, Winstead C and McKoy V 2013 *J. Phys. B: At. Mol. Opt. Phys.* **46** 125201

[27] ETP Equipe Thermodynamique et Plasmas (ETP) model AF151 https://etp-ms.com/
[28] Brunt J H, King G C and Read F H 1977 *J. Phys. B: At. Mol. Opt. Phys.* **10** 1289
[29] ARi Industries, Inc. 1HN040B-16.3 biaxial cable https://ariindustries.biz/
[30] Hughes M, James K E Jr, Childers J G and Khakoo M A 2003 *Meas. Sci. Technol.* **14** 841
[31] Huber K P and Herzberg G 1979 *Molecular Spectra and Molecular Structure* vol 4 (Princeton, NJ: Van Nostrand-Reinhold) pp 162–9
[32] LeClair L and Trajmar S 1996 *J. Phys. B: At. Mol. Opt. Phys.* **29** 5543
[33] Schow E, Hazlett K, Medina C, Vitug G, Childers J G, Bray I and Khakoo M A 2005 *Phys. Rev.* A **72** 062717
[34] Zawadzki M and Khakoo M A 2019 unpublished
[35] Register D F, Trajmar S and Srivastava S K 1980 *Phys. Rev.* A **21** 1134
[36] Khakoo M A, Johnson P V, Ozkay I, Yan P, Trajmar S and Kanik I 2005 *Phys. Rev.* A **71** 062703
[37] Hargreaves L R *et al* 2017 *J. Phys. B: At. Mol. Opt. Phys.* **50** 225203
[38] Hammond P, King G C, Jureta J and Read F H 1985 *J. Phys. B: At. Mol. Opt. Phys.* **18** 2057
[39] Daviel S, Wallbank B, Comer J and Hicks P J 1982 *J. Phys. B: At. Mol. Opt. Phys.* **15** 1929
[40] Gilmore F R, Laher R R and Espy P J 1992 *J. Chem. Phys. Ref. Data* **21** 1005
Laher R private communication
[41] Press W H, Teukosky S A, Vetterling W V and Flannery B P 1988 *Numerical Recipes in C* (Cambridge: Cambridge University Press) ch 14
[42] Nickel J C, Zetner P W, Shen G and Trajmar S 1989 *J. Phys. E: Sci. Instrum.* **22** 730
[43] Zawadzki M *et al* 2018 *Phys. Rev.* A **98** 062704
[44] Hall R and Andric L 1968 *J. Phys. B: At. Mol. Opt. Phys.* **17** 1875
[45] Carr J M *et al* 2012 *Eur. J. Phys.* D **66** 58
[46] Mašín Z, Benda J, Gorfinkiel J D, Harvey A G and Tennyson J 2020 *Comput. Phys. Commun.* **249** 107092
[47] Meltzer T, Tennyson J, Masin Z, Zammit M C, Scarlett L H, Fursa D V and Bray I *J. Phys. B: At. Mol. Opt. Phys.* in preparation
[48] Dora A and Tennyson J 2019 *Quantum Collisions and Confinement of Atomic and Molecular Species, and Photons* (*Springer Proceedings in Physics* vol 230) ed P Deshmukh, E Krishnakumar, S Fritzsche, M Krishnamurthy and S Majumder (Singapore: Springer) p 48
[49] Werner H-J, Knowles P J, Knizia G, Manby F R and Schütz M 2012 MOLPRO, version 2012.1, a package of *ab initio* programs and others, also see https://molpro.net
[50] Faure A, Gorfinkiel J D, Morgan L A and Tennyson J 2002 *Comput. Phys. Commun.* **144** 224
[51] Dora A and Tennyson J 2020 *J. Phys. B: At. Mol. Opt. Phys.* submitted
[52] Baluja K L, Mason N J, Morgan L A and Tennyson J 2000 *J. Phys. B: At. Mol. Opt. Phys.* **33** L677
[53] Lovas F J, Eberhard T, Coursey J S, Kotochigova S A, Chang J, Olsen K and Dragoset R A NIST Standard Reference Database 114 https://nist.gov/pml/diatomic-spectral-database
[54] Nielsen E S, Jørgensen P and Oddershede J 1980 *J. Chem. Phys.* **73** 6238
[55] Darby-Lewis D, Mašín Z and Tennyson J 2017 *J. Phys. B: At. Mol. Opt. Phys.* **50** 175201
[56] Regeta K, Allan M, Winstead C, McKoy V, Mašín Z and Gorfinkiel J D 2016 *J. Chem. Phys.* **144** 024301
[57] Sundholm D, Olsen J and Jorgensen P 1995 *J. Chem. Phys.* **102** 4143
[58] Norcross D W and Padial N T 1982 *Phys. Rev.* A **25** 226
[59] Sanna N and Gianturco F A 1998 *Comput. Phys. Commun.* **114** 142
[60] Rescigno T N and Schneider B I 1992 *Phys. Rev.* A **45** 2894
[61] Zammit M C, Fursa D V, Savage J S and Bray I 2017 *J. Phys. B: At. Mol. Opt. Phys.* **50** 123001
[62] Zammit M C, Savage J S, Fursa D V and Bray I 2017 *Phys. Rev.* A **95** 022708
[63] Gorfinkiel J D and Tennyson J 2004 *J. Phys. B: At. Mol. Opt. Phys.* **37** L343–50
[64] Gorfinkiel J D and Tennyson J 2005 *J. Phys. B: At. Mol. Opt. Phys.* **38** 1607–22